

12-2011

Boundary Element Method (BEM) and Method of Fundamental Solutions (MFS) for the boundary value problems of the 2-D Laplace's equation

Ermes Anthony Salgado-Ibarra
University of Nevada, Las Vegas

Follow this and additional works at: <https://digitalscholarship.unlv.edu/thesesdissertations>



Part of the [Mathematics Commons](#), and the [Partial Differential Equations Commons](#)

Repository Citation

Salgado-Ibarra, Ermes Anthony, "Boundary Element Method (BEM) and Method of Fundamental Solutions (MFS) for the boundary value problems of the 2-D Laplace's equation" (2011). *UNLV Theses, Dissertations, Professional Papers, and Capstones*. 1262.
<https://digitalscholarship.unlv.edu/thesesdissertations/1262>

This Thesis is protected by copyright and/or related rights. It has been brought to you by Digital Scholarship@UNLV with permission from the rights-holder(s). You are free to use this Thesis in any way that is permitted by the copyright and related rights legislation that applies to your use. For other uses you need to obtain permission from the rights-holder(s) directly, unless additional rights are indicated by a Creative Commons license in the record and/or on the work itself.

This Thesis has been accepted for inclusion in UNLV Theses, Dissertations, Professional Papers, and Capstones by an authorized administrator of Digital Scholarship@UNLV. For more information, please contact digitalscholarship@unlv.edu.

Boundary Element Method (BEM) and Method of Fundamental Solutions (MFS)

for the boundary value problems of the 2-D Laplace's equation

By

Ermes Anthony Salgado-Ibarra

Bachelor of Science

UCLA (University of California, Los Angeles)

2004

A thesis submitted in partial fulfillment
of the requirements for the

Master of Science in Mathematical Sciences

Department of Mathematical Sciences
College of Science
The Graduate College

University of Nevada, Las Vegas
December 2011

Copyright © 2011 By Ermes Anthony Salgado-Ibarra

All rights reserved



THE GRADUATE COLLEGE

We recommend the thesis prepared under our supervision by

Ermes Slgado-Ibarra

entitled

Boundary Element Method (BEM) and Method of Fundamental Solutions (MFS) for the Boundary Value Problems of the 2-D Laplace's Equation

be accepted in partial fulfillment of the requirements for the degree of

Master of Science in Mathematical Sciences

Department of Mathematical Sciences

Xin Li, Committee Chair

Monica Neda, Committee Member

Amei Amei, Committee Member

Pushkin Kachroo, Graduate College Representative

Ronald Smith, Ph. D., Vice President for Research and Graduate Studies
and Dean of the Graduate College

December 2011

ABSTRACT

**Boundary Element Method (BEM) and Method of Fundamental Solutions (MFS)
for the boundary value problems of the 2-D Laplace's equation**

By

Ermes A. Salgado-Ibarra

Dr. Li Xin, Examination Committee Chair
Associate Professor of Mathematics
University of Nevada, Las Vegas

In this thesis we study the solution of the two dimensional Laplace equation by the boundary Element method (BEM) and the method of fundamental solutions (MFS). Both the BEM and MFS used to solve boundary value problems involving the Laplace equation 2-D settings. Both methods rely on the use of fundamental solution of the Laplace's equation (the solution of Laplace's equation in the distributional sense). We will contrast and compare the results we get using the BEM with results we get using the MFS.

ACKNOWLEDGEMENTS

I thank my thesis advisor Dr. Xin Li for his very valuable time and patience in guiding me to finish this thesis project. Talking graduate courses from him was a great pleasure also. He is always available to help during his office hours to answer concerns about course material, and thesis material. To many things irrelevant in many ways to me completing my thesis project sooner made it a little hard for me to finish sooner. Also, numerical analysis was not something I was familiar with nor did I ever seriously considered working on a project on any topic related to it. Nevertheless, making an effort to put aside any personal concerns made it possible for for me to see and learn something from a different field in applied mathematics that is very important not just from the point of view of a pure mathematical point of view but also for the treatment of practical problems in the applied sciences that often involve partial differential equations that model them. More often than not there is no other way to get an insight about the solution of such problems without the help of a numerical method. Personally, I hope to pursue a career in astrophysics in the near future or in electrical engineering. I'm sure what I learnt from my thesis project will come in handy in these fields too.

I am very grateful for the all my thesis advisors patience and time in reviewing the material before a final submission. Their time is very valuable to me, as some outside factors such as health, taking classes while trying to finish this project too, etc., also made it a little difficult for me to finish this project sooner. But better latter than never. So my sincerest gratitude for my thesis advisor, and thesis committee members for their patience, and kindness, for their priceless time. I thank you all from the bottom of my heart and best wishes for all of you as part of the UNLV mathematical sciences department and in your personal lives.

TABLE OF CONTENTS

ABSTRACT.....	iii
TABLE OF CONTENTS.....	v
ACKNOWLEDGEMENTS.....	iv
CHAPTER 1 INTRODUCTION Fundamental Solution (of the 2-D Laplace Equation).....	1
1.1 The Fundamental Solution.....	1
1.2 The 2-D δ -function.....	1
1.3 Fundamental Solution.....	8
1.4 The 2-D Laplace Equation.....	8
1.5 Green's Formula.....	11
CHAPTER 2 BOUNDARY ELEMENT METHOD (BEM).....	12
2.1 Description of BEM.....	12
2.2 The boundary value problem.....	14
2.3 Application of the fundamental solution with a singularity to Green's formula.....	15
2.4 Boundary element solution of a boundary value problem for the Laplace equation using linear boundary element.....	27
2.5 Quadratic boundary elements.....	32
2.6 Solution of the Laplace equation using quadratic boundary elements.....	35
CHAPTER 3 Method of fundamental solutions (MFS): Comparison with the 2-D Poisson equation and Laplace's Equations from chapter 2.....	40
3.1 Numerical implementation of the MFS for the Poisson's equation.....	40
3.2 Numerical implementation of the MFS for the Laplace's equation with a Neumann boundary condition for the St.Venant's beam torsion problem in chapter 2.....	47
3.3 Concluding Remarks.....	55
APPENDIX A, LIST OF ABBREVIATIONS.....	61
APPENDIX B LIST OF FIGURES.....	62
REFERENCES.....	63
VITA.....	64

Chapter 1

Fundamental solution of the 2-D Laplace Equation

1.1 Fundamental Solution

To use the BEM to solve boundary value problems we need to transform the boundary value problem into a boundary integral equation. We use the Green's theorem and the concept of the fundamental solution introduced in what follows to describe the transformation process more precisely. The BEM will be used to find a numerical solution to the Laplace partial differential equation in a domain $\Omega \subset \mathbb{R}^m$ where \mathbb{R}^m is the usual m -dimensional Euclidean space ($m=2$, for the rest of the discussion).

1.2 The 2-D δ Function

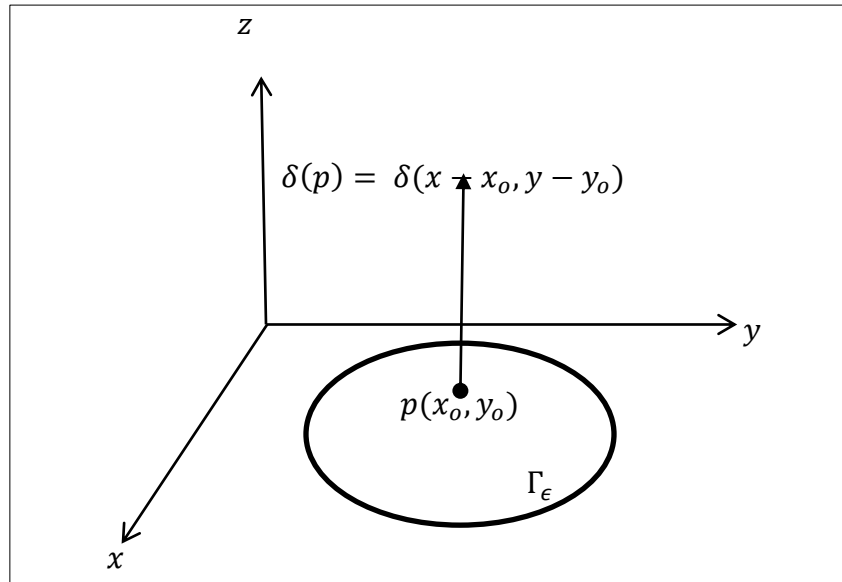
Before we discuss the fundamental solution a brief review of the Dirac delta function in \mathbb{R}^2 denoted by the symbol δ (similar to the case of \mathbb{R}^1 -dimensional space, or the real number line). The Dirac delta function will be used to derive the fundamental solution of the Laplace equation in 2-dimensional Euclidean space. Let L be a linear partial differential operator with constant coefficients in \mathbb{R}^m . $\varphi(p), p \in \mathbb{R}^m$, is called a fundamental solution of L if φ satisfies the equation

$$L(\varphi) = -\delta(p), \quad p \in \mathbb{R}^m \tag{1.2}$$

where the operator L has form $= \sum_{|\alpha| \leq m} a_\alpha D^\alpha$, $\alpha = (\alpha_1, \dots, \alpha_N)$ is a multi-index, α_n 's are non-negative integers, $|\alpha| = \alpha_1 + \dots + \alpha_n$, $a_\alpha = a_{\alpha_1, \alpha_2, \dots, \alpha_N}$ are constant coefficients, and $D^\alpha = \left(\frac{\partial}{\partial x_1}\right)^{\alpha_1} \dots \left(\frac{\partial}{\partial x_N}\right)^{\alpha_N} = \frac{\partial^{|\alpha|}}{\partial x_1^{\alpha_1} \dots \partial x_N^{\alpha_N}}$ and $\delta(p)$ is the Dirac delta function in \mathbb{R}^m . Although strictly speaking, the Dirac delta function is not a function in the ordinary sense of the definition of a function in mathematical jargon, it can be defined as a continuous linear functional (also called a singular distribution) in terms of the weak limit of a sequence of regular functions such as the Gaussian distribution functions, Cauchy distributions, "box" functions, etc., [Lokenath Debanth and Piotr Mikusinsky 2005]. Similar to how the Dirac delta is defined in \mathbb{R}^1 as a weak limit of functions defined on the real line one can define the Dirac delta function in \mathbb{R}^m , for $m \geq 2$ -D spaces. Thus, in the case of a 2-D Euclidean space, let $q(x, y)$ and $p(x_o, y_o)$ represent a pair of moving and fixed points on the x-y plane, respectively, Γ_ϵ a small disk centered at p ; and $A_\epsilon = \epsilon$ the area of the circle (figure 1.1) and define a set of functions denoted by $\delta_\epsilon(q, p)$, where $\epsilon > 0$ by

$$\delta_\epsilon(p, q) = \delta_\epsilon(x - x_o, y - y_o) = \begin{cases} \frac{1}{\epsilon}, & (x, y) \in \Gamma_\epsilon \\ 0, & (x, y) \notin \Gamma_\epsilon \end{cases} \tag{1.2}$$

Figure 1.1: The 2-D δ function



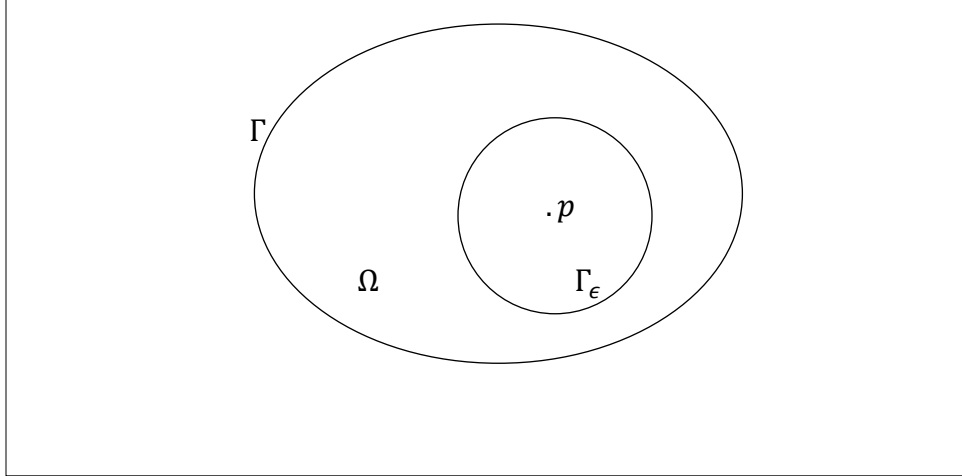
We take the limit of $\delta_\epsilon(q, p)$, as $\epsilon \rightarrow 0$, in equation (1.2) to get

$$\begin{aligned} \delta(q, p) &= \lim_{\epsilon \rightarrow 0} \delta_\epsilon(q, p) = \lim_{\epsilon \rightarrow 0} \delta_\epsilon(x - x_0, y - y_0) \\ &= \delta(x - x_0, y - y_0) = \begin{cases} \infty, & (x, y) = (x_0, y_0) \\ 0, & (x, y) \neq (x_0, y_0) \end{cases} \end{aligned} \quad (1.3)$$

where equation (1.3) defines the Dirac delta function as the weak limit of the functions defined by equation (1.2) for each $\epsilon > 0$, as $\epsilon \rightarrow 0$.

Next, draw a 2-D region Ω that encloses p (figure 1.2) and let $d\Omega$ denote an infinitesimal area element of this region, and Γ_ϵ a disk centered at p is a neighborhood of p within Ω of area ϵ . Note that in the following integral formulas we write $d\Gamma$ to denote an infinitesimal boundary element of the boundary of domain Ω , which we write as $\partial\Omega = \Gamma$.

Figure 1.2: A small disk Γ_ϵ enclosing point p within Ω



Then the integral of the 2-D δ function over the region Ω gives

$$\begin{aligned}
 \int_{\Omega} \delta(p, q) d\Omega &= \int_{\Omega} \delta(x - x_o, y - y_o) d\Omega \\
 &= \lim_{\epsilon \rightarrow 0} \int_{\Gamma_\epsilon} \delta_\epsilon(x - x_o, y - y_o) d\Gamma_\epsilon \\
 &= \lim_{\epsilon \rightarrow 0} \int_{\Gamma_\epsilon} \frac{d\Gamma_\epsilon}{\epsilon} = \lim_{\epsilon \rightarrow 0} \frac{\epsilon}{\epsilon} = 1.
 \end{aligned} \tag{1.4}$$

The integral here is over region Ω , a 2-D domain but for simplicity, we use a single rather than a double integral symbol to represent the domain integral. For convenience, $\delta(q, p)$ is denoted by $\delta_p(q)$, which will represent a 2-D δ function centered at fixed point p in Ω . Thus, definition (1.3) and the integral (1.4) are rewritten as

$$\delta_p(q) = \begin{cases} \infty, & \text{if the moving point } q \text{ is at } p, \\ 0, & \text{for } q \neq p, \end{cases} \quad (1.5)$$

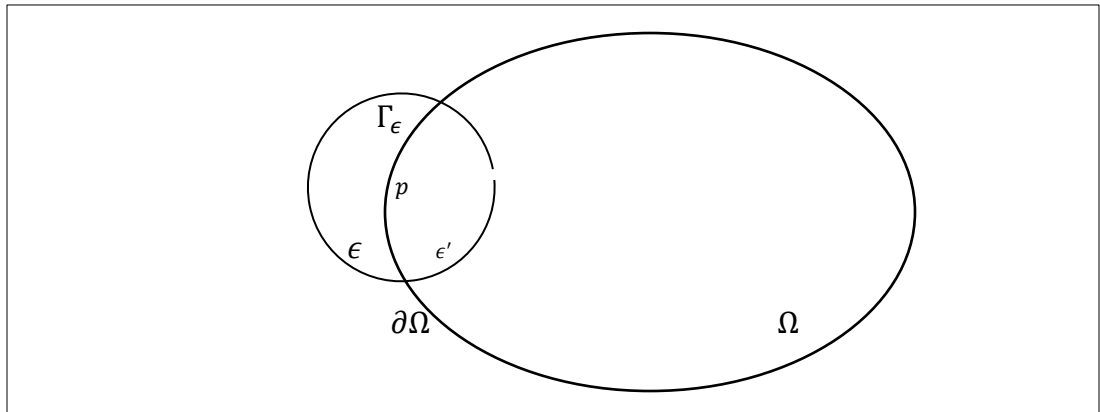
and

$$\int_{\Omega} \delta_p(q) d\Omega = 1, \quad p \text{ is inside } \Omega. \quad (1.6)$$

If p is on the (smooth) boundary $\partial\Omega$ of region Ω (Figure 1.3), then the disk Γ_{ϵ} surrounding p (the center of Γ_{ϵ}) is divided into two parts by $\partial\Omega$. Namely, the portion of Γ_{ϵ} within Ω (forming a semicircular disk $\Gamma_{\epsilon'}$, of approximate area $\frac{1}{2}\epsilon$) and the portion of Γ_{ϵ} outside of Ω . Hence,

$$\begin{aligned} \int_{\Omega} \delta_p(q) d\Omega &= \lim_{\epsilon \rightarrow 0} \int_{\Gamma_{\epsilon'}} \delta_{p_{\epsilon'}}(q) d\Gamma_{\epsilon'} = \lim_{\epsilon \rightarrow 0} \int_{\Gamma_{\epsilon'}} \frac{d\Gamma_{\epsilon'}}{\epsilon} \\ &= \lim_{\epsilon \rightarrow 0} \frac{\epsilon'}{\epsilon} = \frac{1}{2}. \end{aligned} \quad (1.7)$$

Figure 1.3: Point $p \in \partial\Omega$, the (smooth) boundary of Ω ; ϵ' is the portion of disk Γ_{ϵ} within Ω centered at p forming a semicircular disk $\Gamma_{\epsilon'}$ of area $\epsilon' = \frac{1}{2}\epsilon$

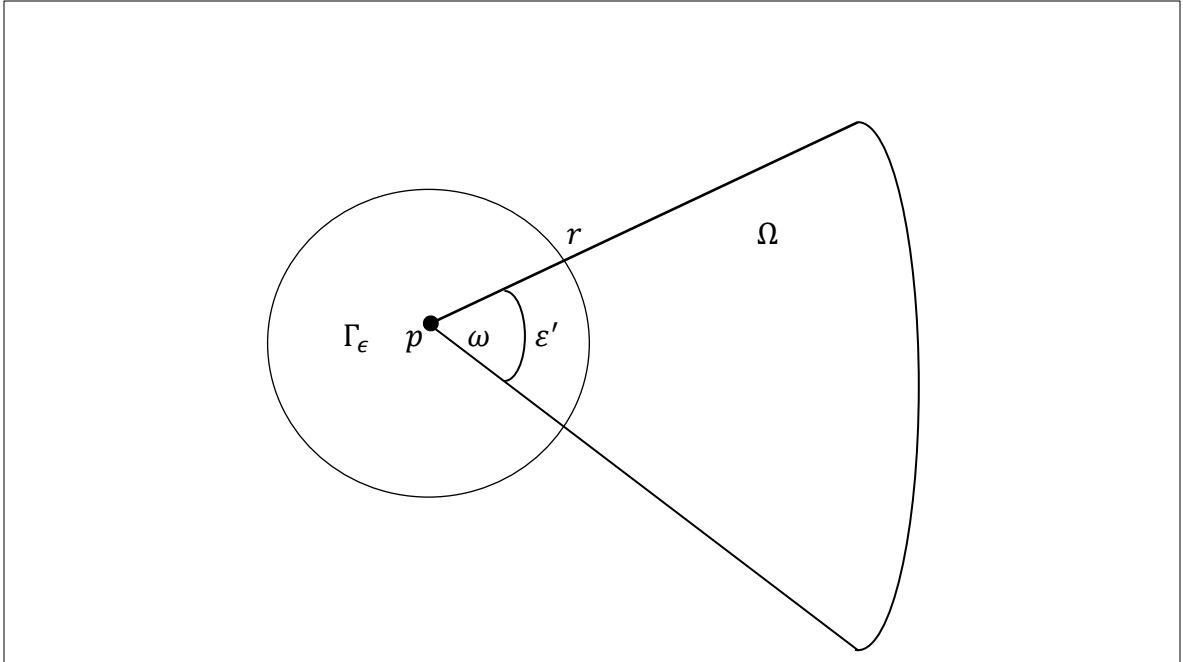


Note that the portion of Γ_ϵ outside of Ω makes no contribution to the integral of the Dirac-delta function and only the portion of the semicircular disk $\Gamma_{\epsilon'}$ makes any nonzero contribution to the integral in equation (1.7). In the context of equation (1.7) the Dirac delta function is said to have compact support within domain or 2-D region Ω (recall that the support of a function is the closure of a set of points in a domain outside of which it vanishes). If the boundary at p is not smooth (figure 1.4) then the integral is given by

$$\int_{\Omega} \delta_p(q) d\Omega = \lim_{\epsilon \rightarrow 0} \frac{\epsilon'}{\epsilon} = \lim_{\epsilon \rightarrow 0} \frac{\frac{\omega}{2} r^2}{\pi r^2} = \frac{\omega}{2\pi} \quad (1.8)$$

where r is the radius of the circle and ω is the angle included within $\partial\Omega$ at p ; i.e., ω is the 2-D solid angle made by p against the boundary $\partial\Omega$ of region Ω and $d\Omega$ reduces to $d\Gamma_{\epsilon'}$ the only part of Ω that will contribute to the integral in equation (1.8). Notice that equation (1.8) is the general case of equations (1.6) and (1.7). Thus, if p is entirely inside Ω then $\omega = 2\pi$ and equation (1.6) results from using equation (1.7). Similarly, if $p \in \partial\Omega$ (a smooth boundary) then $\omega = \pi$ and equation (1.7) is also the result of using equation (1.8).

Figure 1.4: The point p is on the broken boundary, r is the radius of the small disk Γ_ϵ of area ϵ and ω is the angle included within $\partial\Omega$ at p . Only the portion of the disk $\Gamma_{\epsilon'}$ of area ϵ' contributes to the integral in equation (1.8)



More generally, we can use the properties of the Dirac delta function to calculate the value of a 2-D continuous function $u(x, y)$ at a point p inside a 2-D domain Ω and its boundary $\partial\Omega = \Gamma$. Analogous to the 1-D δ function it can be shown that the value of u (provided u is continuous in domain Ω and on its boundary) is given by the following formulas:

$$\int_{\Omega} u(x, y) \delta_p(q) d\Omega = \begin{cases} u_p(q), & \text{if } p \text{ is inside domain} \\ u_p(q)/2, & \text{if } p \text{ is on smooth boundary } \Gamma \\ u_p(q)\omega/2\pi, & \text{if } p \text{ is on a non-smooth boundary } \Gamma. \end{cases} \quad (1.9)$$

It can be shown [Debanath and Mikusinski 2005] that the above result can be generalized to the case of higher dimensions than 2 for continuous functions u in \mathbb{R}^m with compact support (i.e. the closure of the set of points $x \in \mathbb{R}^m$ outside where u vanishes).

1.3 Fundamental Solution

To use the BEM to solve boundary value problems we must transform the problem into an equivalent boundary integral equation problem. The use of the fundamental solution (i.e., the Green's function) and Green's integral theorems are very useful tools for this purpose. We discuss next the fundamental solution to the 2-D Laplace partial differential equation.

1.4 2-D Laplace Equation

According to the definition (equation (1.1)), the fundamental solution φ of the 2-D Laplace equation

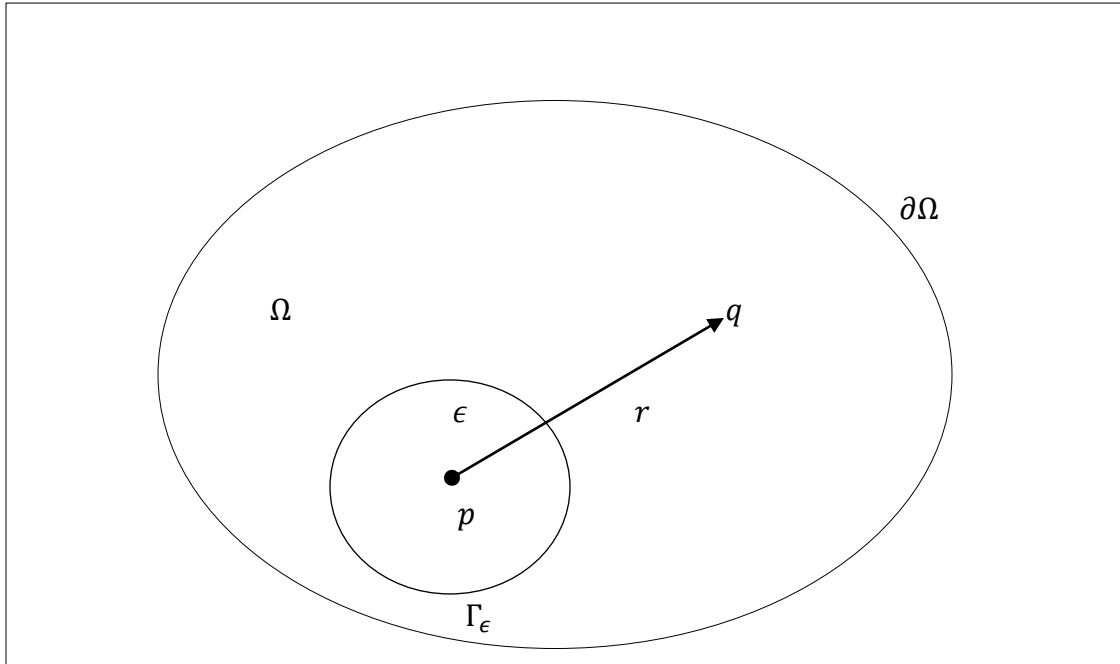
$$\nabla^2 u = \frac{\partial^2 u}{\partial x^2} + \frac{\partial^2 u}{\partial y^2}$$

should satisfy

$$\nabla^2 \varphi = -\delta_p(q), \tag{1.10}$$

where $\delta_p(q)$ is the Dirac delta function centered at a point $p \in \Omega$ in a 2-D domain (figure 1.5).

Figure 1.5: A 2-D domain Ω with boundary $\partial\Omega$



Taking p as the origin and expanding equation (1.9) in polar coordinates, we analyze the circularly symmetric solution $\varphi = \varphi(r)$. Thus, with φ only dependent only of r and $\delta_p(q) = 0$, if $r \neq 0$, equation (1.9) can be written in the form

$$\nabla^2 \varphi = \frac{1}{r} \frac{d}{dr} \left(r \frac{d\varphi}{dr} \right) = 0, \quad r \neq 0. \quad (1.11)$$

The integral of (1.11) is calculated directly to give the general solution φ in the form

$$\varphi = A \ln r + B \quad \text{for } r \neq 0, \quad (1.12)$$

where A and B are integration constants. Clearly φ satisfies

$$\nabla^2 \varphi = \infty \quad \text{for } r = 0. \quad (1.13)$$

The surface integral of $\nabla^2\varphi$ should also satisfy

$$\int_{\Omega} \nabla^2\varphi d\Omega = - \int_{\Omega} \delta_p(q) d\Omega = -1 \quad (1.14)$$

where Ω is an arbitrary 2-D domain surrounding p . Again, let Γ_{ϵ} be a small disk centered at p (Figure 1.5) of area $A_{\epsilon} = \epsilon$. Then using the divergence theorem the integral in (1.14) is transformed into a line integral over the boundary of disk Γ_{ϵ} , which we denote by Γ . Thus,

$$\begin{aligned} \int_{\Omega} \nabla^2\varphi d\Omega &= \int_{\Gamma_{\epsilon}} \nabla^2\varphi d\Omega = \int_{\Gamma_{\epsilon}} \nabla \cdot \nabla\varphi d\Omega \\ &= \oint_{\Gamma_{\epsilon}} (\nabla\varphi)_n d\Gamma = \oint_{\Gamma_{\epsilon}} \frac{d\varphi}{dr} d\Gamma = \oint_{\Gamma_{\epsilon}} \frac{A}{r} d\Gamma \end{aligned}$$

Hence, we get

$$\frac{A}{r} \oint_{\Gamma_{\epsilon}} d\Gamma = \frac{A}{r} 2\pi r = 2\pi A, \quad (1.15)$$

where $(\nabla\varphi)_n$ is the projection of the normal component of the gradient of φ along the contour $\partial\Gamma_{\epsilon}$. Thus, substituting (1.15) into equation (1.14) yields $A = -\frac{1}{2\pi}$. Setting $B = 0$ in equation (1.12) we obtain the fundamental solution to the 2-D Laplace equation,

$$\varphi = \frac{1}{2\pi} \ln \frac{1}{r}. \quad (1.16)$$

The fundamental solution to the Laplace equation has a physical interpretation. From electromagnetic field theory, it can be shown that the electric potential generated at a point q by a line of charge at a point p with unit linear charge density is $u = \frac{1}{2\pi} \ln \frac{1}{r}$

(omitting any dielectric constant), where r is the distance from p to q where point p is often called the source point and q the field point, or point at which we wish to measure the effect of the source a distance r away from it in a 2-D, or 3-D region of space in which the field due to the source acts (electromagnetic, gravitational, fields for example).

1.5 Green's Formula

In transforming boundary value problems to integral equation problems, Green's formula is a very useful tool. We state the result. It will be very useful in the derivation of latter results to follow. Suppose u and v are continuous functions in a domain $\Omega \subset \mathbb{R}^2$, with continuous first and second derivatives in Ω as well. Then functions u and v satisfy the Green's formula,

$$\int_{\Omega} (u\nabla^2 v - v\nabla^2 u) d\Omega = \oint_{\Gamma} \left(u \frac{\partial v}{\partial n} - v \frac{\partial u}{\partial n} \right) d\Gamma, \quad (1.17)$$

where $\Gamma = \partial\Omega$ is the boundary of domain Ω and $\frac{\partial u}{\partial n}$, and $\frac{\partial v}{\partial n}$ are the outward normal derivatives of v and u , respectively on the boundary of domain Ω .

Chapter 2

Boundary Element Method (BEM)

2.1 Description of BEM

As a numerical method, the boundary element method, or BEM, is a more recently developed numerical method used to find approximate solutions to boundary value problems. Prior to its development there was so called boundary integral equation methods in which the boundary value problem of a partial differential equation was transformed into an integral equation over the boundary of the region by the use of equations like Green's formula (equation (1.16)). The boundary element method complements the finite element method (FEM) method to solve boundary value problems. The main difference between the boundary element method and the finite element method is that the finite element method is a regional method. This means that the whole region of interest is discretized. If the regions are not regular and automatic discretization techniques cannot be used, an artificial method must be used to discretize the region, or domain characterizing the geometry of the problem, or the type of partial differential equation that needs to be solved for some particular problem. Thus, the preparation and input of data used to model a boundary value problem into a computer may become a very complex task. For example, the number of element nodes in the

FEM can become so large that the ultimate system of linear equations is huge. The boundary element method divides only the boundary, or boundaries of the region of interest into elements. This diminishes the dimensionality of the problem. The 3-D problem becomes a 2-D problem, a 2-D problem, likewise, becomes a 1-D problem. Hence, input of data to model the problem into a computer becomes a less complex task as the number of resulting algebraic equations involved is significantly reduced.

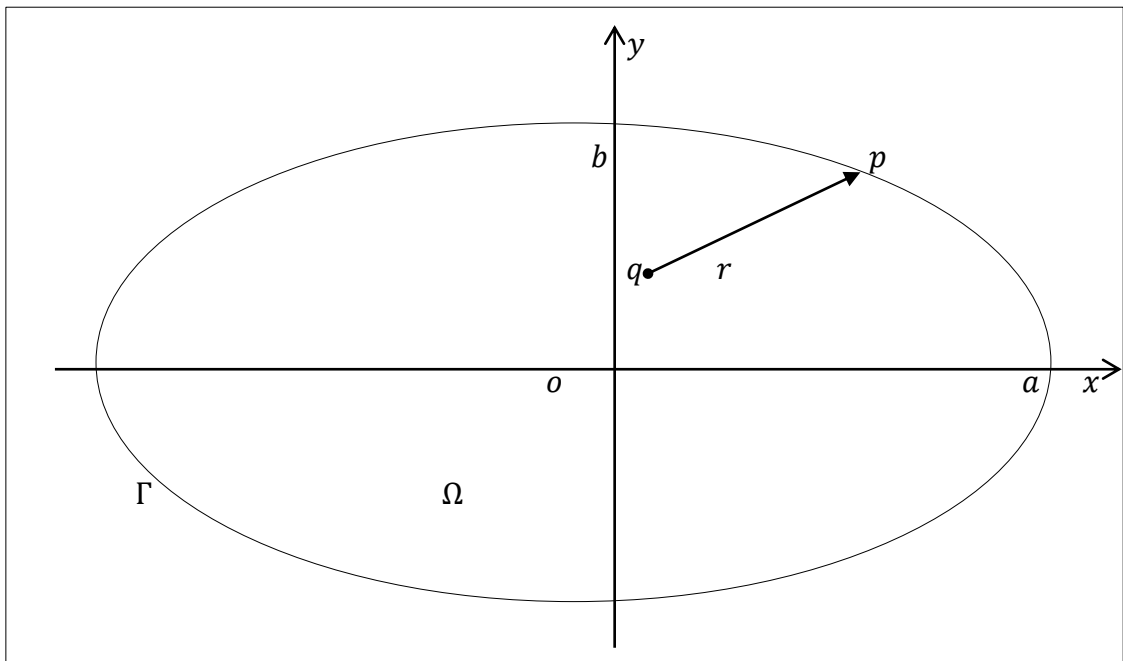
The basic steps in the process of solving a boundary value problem using the BEM are as follows:

- 1) Determine a partial differential equation and boundary conditions (also, any initial conditions) of the boundary value problem.
- 2) Transform the region (by a region we mean a domain in 2-D, or 3-D space), the partial differential equations, and boundary conditions into a set of boundary integral equations. The main mathematical tool for this transformation is the Green's formula as mentioned above.
- 3) Similar to the FEM, we divide the boundary of the domain into finite elements and assume a zero, or linear, second, or higher order interpolation over an element as appropriate for the particular domain of interest. Add up the integrals over each element, such that the boundary integral equation is discretized into a system of linear equations. Solving the resulting system of equations, we obtain a function value at each node or the numerical approximation to the solution of our boundary value problem.

2.2 The boundary value problem

Let Ω be a two-dimensional domain bounded by an ellipse in the x - y plane with equation given by $\frac{x^2}{a^2} + \frac{y^2}{b^2} = 1$, where a is the semi-major axis, and b is the semi-minor axis of the ellipse (figure 2.1).

Figure 2.1: A domain Ω in the x - y plane (the interior of an ellipse) with boundary Γ



Consider the following boundary value problem of the Laplace equation in a domain Ω of \mathbb{R}^2 defined by

$$\Delta u(x) = 0, \quad x \in \Omega, \quad (2.1)$$

$$Bu(x) = f(x), \quad x \in \Gamma, \quad (2.2)$$

where $x = (x, y)$, $\Delta = \nabla^2$ the well-known Laplacian operator which can be given in polar, Cartesian, and other coordinate systems suitable for the problem under is also a (boundary) linear differential operator that acts on $u(x)$ to yield a Dirichlet, Neumann, or Robin (mixed) boundary condition that the solution $u(x)$ must satisfy on the boundary of a given 2-D domain.

2.3 Application of the fundamental solution with a singularity to the Green's formula

Let p be a point on the boundary Γ of a 2-D domain Ω , where we wish to calculate the solution $u(x)$ of the Laplace equation for the boundary value problem given by equations (2.1), and (2.2). Take

$$\varphi = \frac{1}{2\pi} \ln \frac{1}{r} \quad (2.3)$$

as the fundamental solution of the Laplace equation (derived in chapter 1), substituting u and φ into the Green's formula in equation (1.16) yields

$$\int_{\Omega} (u \nabla^2 \varphi - \varphi \nabla^2 u) d\Omega = \oint_{\Gamma} \left(u \frac{\partial \varphi}{\partial n} - \varphi \frac{\partial u}{\partial n} \right) d\Gamma, \quad (2.4)$$

where Γ is the boundary of 2-D domain Ω (Figure 2.1) and r is the distance from a point $q \in \Omega$ to the point $p \in \Gamma$. Note that both p , and q can be inside the domain Ω , but when applying the BEM one point or the other becomes a boundary point. Thus, the fundamental solution φ given by equation (2.4) has a singularity at p , since

$r = \sqrt{|q - p|}$ (the Euclidean distance from p to q) and $\lim_{q \rightarrow p} r = 0$. Hence, φ becomes

undefined at $p \in \Gamma$. However, if the Dirac 2-D Dirac delta function is used i.e. φ satisfies

$\nabla^2 \varphi = -\delta_p(q)$, and since $\nabla^2 u = \Delta u = 0$ (equation (2.1)), the left hand side of equation

(2.4) gives

$$\int_{\Omega} (u \nabla^2 \varphi - \varphi \nabla^2 u) d\Omega = \int_{\Omega} [-u(q) \delta_p(q)] d\Omega. \quad (2.5)$$

By the integral properties of the δ function if q is inside the region Ω , then

$\int_{\Omega} u [-\delta_p(q)] d\Omega = -u_p$, where u_p is the value of u at $p \in \Omega$. Hence, we have

$$u_p = -\oint_{\Gamma} \left(u \frac{\partial \varphi}{\partial n} - \varphi \frac{\partial u}{\partial n} \right) d\Gamma = \oint_{\Gamma} \left[u \frac{\cos(r,n)}{2\pi r} + \frac{\partial u}{\partial n} \frac{1}{2\pi} \ln \frac{1}{r} \right] d\Gamma. \quad (2.6)$$

Thus, the fundamental solution with a singularity is still applicable to Green's formula in spite of the restrictions imposed on u , and φ about continuity and differentiability of first and second derivatives of these functions if they are to satisfy the Green's formula for any point p inside domain Ω and its boundary Γ .

Equation (2.6) sets up a relation between u at p in domain Ω with u and its normal derivative $\frac{\partial u}{\partial n}$ on the boundary Γ of domain Ω . However, only u is known in the given boundary value problem; $\frac{\partial u}{\partial n}$ is unknown. In this case, equation (2.6) cannot be used to calculate u on Ω . We first must move q onto Γ , thus, from equation (1.9), using the Dirac δ function, the integral on the right hand side of equation (2.5) is given by

$$\int_{\Omega} [-u(q) \delta_p(q)] d\Omega = -\frac{\omega_q}{2\pi} u_p \quad p \in \Omega, \quad (2.7)$$

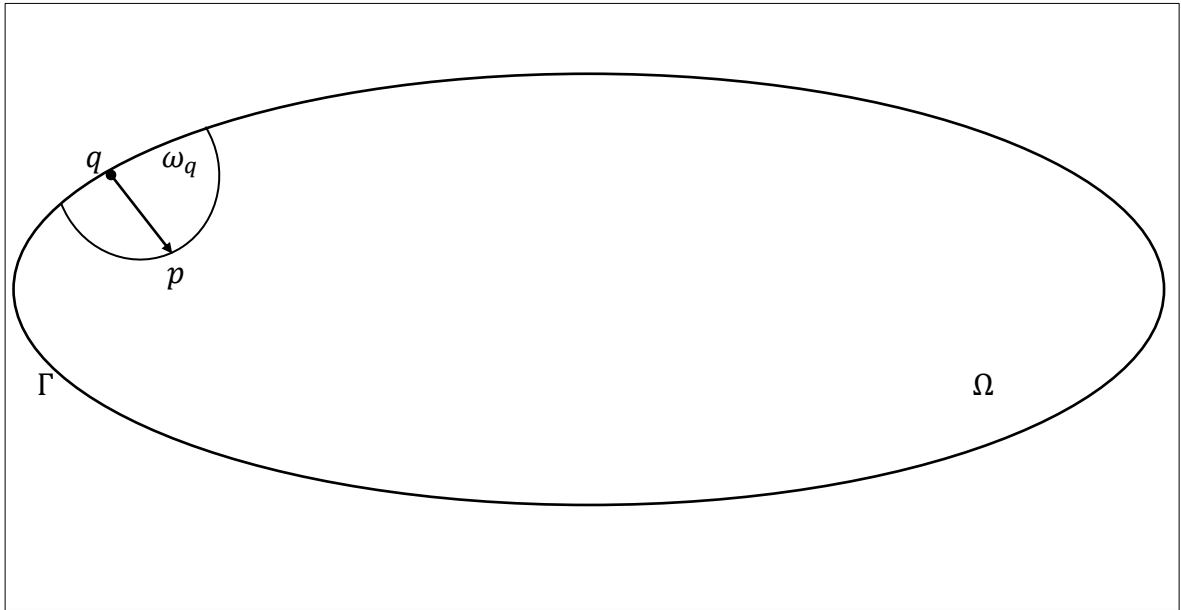
where ω_q the angle is subtended domain by Ω at $q \in \Gamma$ (Figure 2.2). That is, when moving $q \in \Omega$ onto Γ equation (2.6) becomes

$$\frac{\omega_q}{2\pi} u_p = - \oint_{\Gamma} \left(u_q \frac{\partial \varphi}{\partial n} - \varphi \frac{\partial u_q}{\partial n} \right) d\Gamma = \oint_{\Gamma} \left[u_q \frac{\cos(r,n)}{2\pi r} + \frac{\partial u_q}{\partial n} \frac{1}{2\pi} \ln \frac{1}{r} \right] d\Gamma, p \in \Omega, \quad (2.8)$$

respectively, are the values of u in Ω for any $p \in \Omega$. Thus, we obtain a boundary integral equation that sets up a relationship between u and its (outward) normal derivative $\frac{\partial u}{\partial n}$ for a point p on the boundary of domain Ω . Since u is given by the

conditions of the boundary value problem in equation (2.1), $\frac{\partial u}{\partial n}$ can be calculated using the BEM. Hence, by substituting u and $\frac{\partial u}{\partial n}$ at any point $p \in \Omega$ can be calculated.

Figure 2.2: Point q on a smooth boundary Γ of a 2-D domain Ω subtending an angle ω_q against the boundary with respect to q from some point p inside the domain

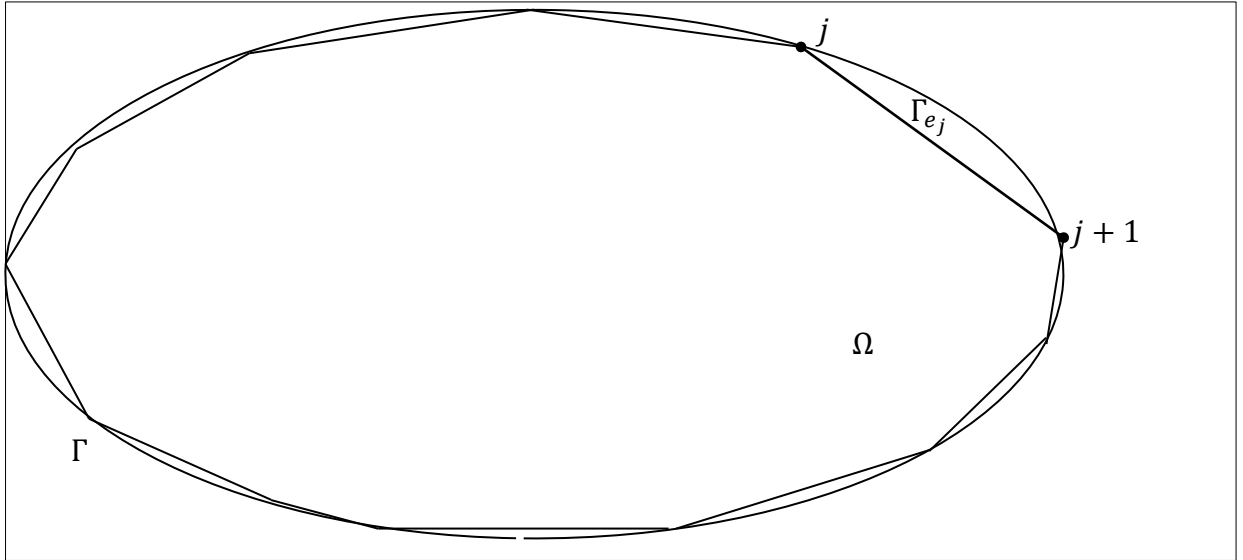


Application of the BEM method:

To solve equation (2.6) we first divide the boundary Γ into many boundary subelements of Γ . Next, u must be interpolated across each element. This can be done by using shape, or basis functions as explained in the steps describing how to carry out the BEM method. The shape functions can be zero order (constant), or first order (linear), or second order (quadratic), or third order (cubic), or even higher order shape functions. Although accuracy may increase with higher order interpolation schemes so will the number of nodes needed to divide the boundary. In the BEM each node has a corresponding linear equation tied to it. Thus, the resulting number of linear equations involved in solving for u will increase as the order of the interpolation scheme to approximate u across each element increases. This, of course, will mean that more time and more memory will be consumed by the computing device being used to carry out the calculations, etc. To understand some specifics, we next explain some interpolation schemes. For simplicity the discussion is limited to the use of linear and quadratic basis functions as the main interpolation schemes to be used in the solution of some boundary value problems that will be dealt with in this thesis paper.

Linear interpolation.— Using the steps described to carry out the BEM we first divide the boundary Γ of domain Ω into $n - 1$ linear elements by n nodes (figure 2.3).

Figure 2.3: A linear boundary element Γ_{e_j} with two endpoints j and $j + 1$



The length of each element should satisfy the following two requirements:

(i) in each element the geometric variation is linear, i.e. it can be described by a linear function and

(ii) the variations in u and $\frac{\partial u}{\partial n}$ are also linear. Let Γ_{e_j} represent a linear element of the subdivision of Γ , where $j = 1, \dots, n - 1$. Decomposing the boundary integral of equation (2.8) into a sum of integrals over each element, the equation for each node i can be rewritten as

$$\frac{\omega_i}{2\pi} u_i = \sum_{j=1}^{n-1} \int_{\Gamma_{e_j}} \left[u \frac{\cos(r,n)}{2\pi r} + \frac{\partial u}{\partial n} \frac{1}{2\pi} \ln \frac{1}{r} \right] \quad (i = 1, \dots, n, \text{ nodes}) \quad (2.9)$$

The node indices for two successive endpoints of an element are, for example, j and $j + 1$; where the first and second end points of an element has coordinates (x_j, y_j) , (x_{j+1}, y_{j+1}) , and values of u , and its normal derivative at these coordinates are denoted by u_j , u_{j+1} , $(\frac{\partial u}{\partial n})_j$, and $(\frac{\partial u}{\partial n})_{j+1}$, respectively. The linear interpolation is carried out using linear isoperimetric elements [Rao 1998]. This means we use local element coordinates to perform integrations over each element by Gaussian quadrature methods that depend on the order of the interpolation scheme. In this case the variables of the problem, u and the local coordinates of a point (x, y) on each element Γ_{e_j} will be expressed as functions of an identical parameter ξ in terms of linear, and quadratic shape functions as explained in what follows. The shape functions used will be based on the Lagrange's interpolation polynomial method [Rao 1982]. For $1 \leq j \leq n - 1$ linear elements, and $i = 1, \dots, n$ nodes, define the shape functions as follows,

$$N_j(\xi) = 1 - \xi, \quad N_{j+1}(\xi) = \xi, \quad (0 \leq \xi \leq 1). \quad (2.10)$$

The shape, or basis functions N_j and N_{j+1} in the equations in (2.10) have the following characteristics:

N_j and N_{j+1} are linear functions of $\xi = \xi_j, 1 \leq j \leq n - 1$, where

$$\sum_{l=j}^{j+1} N_l = 1; \quad N_l(\xi_j) = \delta_{lj} = \begin{cases} 1, & l = j \\ 0, & l \neq j \end{cases} \quad (2.11)$$

where δ_{lj} is the Kronecker delta function. The parameter ξ in the above equations represents a coordinate on the isoperimetric element. A single number representing the

x and y coordinates of a point in a 2-D domain, or on its boundary. If we are dealing with a surface in 3-D Euclidean space for example, two such parameters would be used to approximate the surface in the neighborhood of a point lying on the surface. Hence the number of local coordinates is reduced by one, by using the method of isoperimetric elements to represent the local geometry of a problem domain.

Thus, on each boundary element Γ_{e_j} of Γ (being treated as a linear isoperimetric element) locally, each element is assumed to be a straight line segment, and variations in the variables and coordinates are assumed to be linear; all equations used in the linear interpolation expressed in terms of the linear shape functions in equations (2.10).

That is, to interpolate within each element we set u , x , y , and $\frac{\partial u}{\partial n}$ equal to

$$u = \sum_{l=j}^{j+1} N_l u_l, \quad \frac{\partial u}{\partial n} = \sum_{l=j}^{j+1} N_l \left(\frac{\partial u}{\partial n} \right)_l,$$

$$x = \sum_{l=j}^{j+1} N_l x_l, \quad y = \sum_{l=j}^{j+1} N_l y_l, \quad (j = 1, \dots, n - 1). \quad (2.12)$$

The integrals over each element Γ_{e_j} are,

$$\int_{\Gamma_{e_j}} u \frac{\cos(r,n)}{2\pi r} d\Gamma = \sum_{l=j}^{j+1} \int_{\Gamma_{e_j}} (N_l(\xi) \frac{\cos(r,n)}{2\pi r} d\Gamma) u_l = \sum_{l=j}^{j+1} f_{jl} u_l \quad (2.13)$$

and,

$$\int_{\Gamma_{e_j}} \frac{\partial u}{\partial n} \frac{1}{2\pi} \ln \frac{1}{r} d\Gamma = \sum_{l=j}^{j+1} \left(\int_{\Gamma_{e_j}} N_l(\xi) \frac{1}{2\pi} \ln \frac{1}{r} d\Gamma \right) \left(\frac{\partial u}{\partial n} \right)_l = \sum_{l=j}^{j+1} d_{jl} \left(\frac{\partial u}{\partial n} \right)_l \quad (2.14)$$

$$f_{jl} = \int_{\Gamma_{e_j}} N_l(\xi) \frac{\cos(r,n)}{2\pi r} d\Gamma, \quad d_{jl} = \int_{\Gamma_{e_j}} N_l(\xi) \frac{1}{2\pi} \ln \frac{1}{r} d\Gamma, \quad (2.15)$$

where $1 \leq j \leq n - 1$, and $1 \leq l \leq n$.

The integrals in equations (2.13) and (2.14) can be calculated using Gaussian quadrature. The number of Gaussian points in each element is related to the degree of variation within the integrand. In Gaussian quadrature the integrals are rewritten as a linear combination of the shape functions N_l evaluated at integration points within each element Γ_{e_l} , where $\xi = \xi_q \in \Gamma_{e_l}$. Four Gaussian points are usually enough for the integrals such as given by equation (2.13). In Gaussian quadrature form these integrals are rewritten as

$$f_{jl} = \int_{\Gamma_{e_j}} N_l(\xi) \frac{\cos(r,n)}{2\pi r} d\Gamma = \sum_{q=1}^4 N_l(\xi_q) \frac{\cos(r_{iq},n)}{2\pi r_{iq}} \omega_q L_q \quad (2.16)$$

and

$$d_{jl} = \int_{\Gamma_{e_j}} N_l(\xi) \frac{1}{2\pi} \ln \frac{1}{r} d\Gamma = \sum_{q=1}^4 N_l(\xi_q) \frac{1}{2\pi} \ln \frac{1}{r_{iq}} \omega_q L_q, \quad (2.17)$$

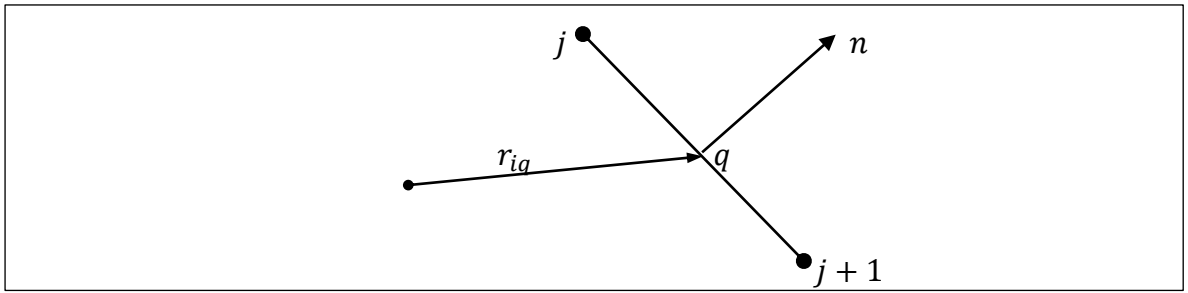
where r_{iq} is the distance from the i -th node to the integration point q on the element Γ_{e_j} (figure 2.4). The coordinates of the Gaussian integration points q are given by

$$x_q = \sum_{l=j}^{j+1} N_l(\xi_q) x_l, \quad y_q = \sum_{l=j}^{j+1} N_l(\xi_q) y_l \quad (2.18)$$

where $\cos(r_{iq}, n)$ is the cosine of the angle between r_{iq} and the outward unit normal vector n to subelement Γ_{e_j} of Γ , the ω_q weights used in integration by the Gaussian

quadrature method , and L_q the length of boundary element Γ_{e_j} as measured from a quadrature point q lying on this element. The values of ξ_q and ω_q for a four point Gaussian integration are given in special tables [Brebbia 1978].

Figure 2.4: Distance from node i to integration point $q = r_{iq}$, for a linear element Γ_{e_j} ; n is a unit outward normal vector to the linear boundary element Γ_{e_j} .



If a node i belongs to an element Γ_{e_i} (i.e., it coincides with j or $j + 1$ (figure 2.5)) then there will exist a singularity as r goes to zero. Thus, the integrands $\frac{\cos(r,n)}{r}$ and $\ln \frac{1}{r}$ are singular but the integrals f_{ij} , f_{ik} , d_{ij} and $d_{i,j+1}$ still exist. The values of these are found to be

$$f_{ij} = \int_{\Gamma_{e_j}} N_j(\xi) \frac{\cos(r,n)}{2\pi r} d\Gamma = 0, f_{ik} = \int_{\Gamma_{e_j}} N_{j+1}(\xi) \frac{\cos(r,n)}{2\pi r} d\Gamma = 0, \quad (2.19)$$

since $\cos(r,n) = \cos \frac{\pi}{2} = 0$, and where $k = j + 1$.

We also get,

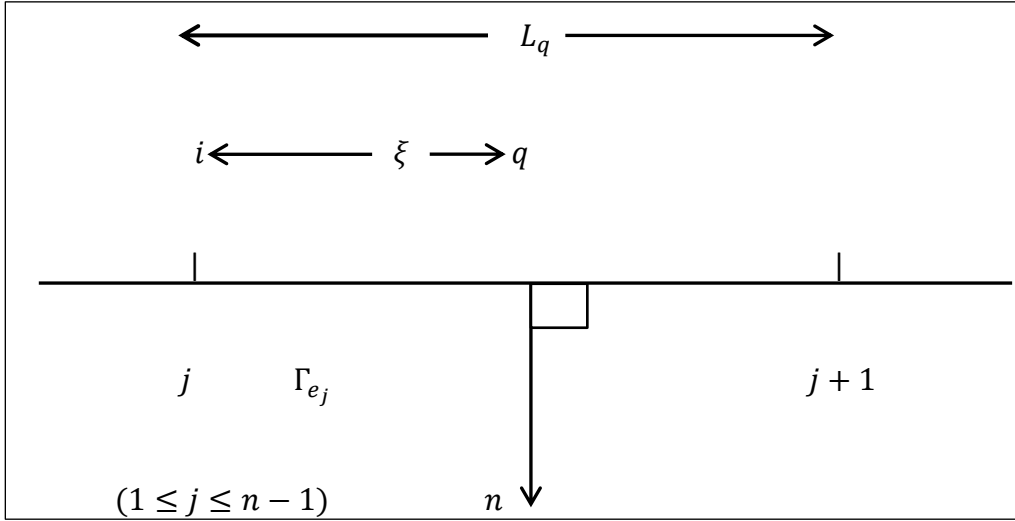
$$d_{ij} = \int_{\Gamma_{e_j}} N_j(\xi) \frac{1}{2\pi} \ln \frac{1}{\xi} d\xi = \int_0^{L_q} \frac{L_q - \xi}{L_q} \frac{1}{2\pi} \ln \frac{1}{\xi} d\xi = \frac{L_q}{4\pi} \left(\frac{3}{2} - \ln L_q \right), \quad (2.20)$$

where $N_j = \frac{L_q - \xi}{L_q}$, and

$$d_{ik} = \int_{\Gamma_{e_j}} N_{j+1}(\xi) \frac{1}{2\pi} \ln \frac{1}{\xi} d\xi = \int_0^{L_q} \frac{\xi}{L_q} \frac{1}{2\pi} \ln \frac{1}{\xi} d\xi = \frac{L_q}{4\pi} \left(\frac{1}{2} - \ln L_q \right). \quad (2.21)$$

where $N_{j+1} = \frac{\xi}{L_q}$, and $k = j + 1$ (for the end point of the j -th boundary element).

Figure 2.5: For singular linear boundary element Γ_{e_j} , L_q is fixed for some fixed quadrature point at node i ; $j \leq \xi_i = \xi \leq j + 1$, and $1 \leq i \leq n$, along $d\Gamma = d\xi$.



Thus, if Γ_{e_j} contains node i , the above formulas are used to calculate f_{ij} , f_{ik} , d_{ij} , and d_{ik} . Otherwise, we need to use the equations (2.12) and (2.13). Before summing the integral (2.9) over each element note that equations (2.12), and (2.13) can be written in terms of matrices that can be expanded into n rows or n columns:

$$\begin{aligned} \sum_{l=j}^{j+1} f_{il} u_l &= f_{ij} u_j + f_{i,k} u_k \\ &= (0, \dots, f_{ij}, f_{ik}, 0, \dots, 0) \cdot (u_1, \dots, u_j, u_k, \dots, u_n)^T \end{aligned} \quad (2.22)$$

and,

$$\begin{aligned} \sum_{l=j}^{j+1} d_{il} \left(\frac{\partial u}{\partial n} \right)_l &= d_{ij} \left(\frac{\partial u}{\partial n} \right)_j + \left(\frac{\partial u}{\partial n} \right)_k d_{ik} \\ &= (0, \dots, d_{ij}, d_{ik}, 0, \dots, 0) \cdot \left[\left(\frac{\partial u}{\partial n} \right)_1, \dots, \left(\frac{\partial u}{\partial n} \right)_j, \left(\frac{\partial u}{\partial n} \right)_k, \dots, \left(\frac{\partial u}{\partial n} \right)_n \right]^T, \end{aligned} \quad (2.23)$$

where $j = 1, \dots, n-1$, $i = 1, \dots, n$, and $k = j+1$ in equations (2.21) and (2.22) and $f_{il} = 0$ for $i \neq j$, and similar results hold for d_{il} .

Now let $\mathbf{F}_{ij} = (0, \dots, f_{ij}, f_{ik}, 0, \dots, 0)$, $\mathbf{D}_{ij} = (0, \dots, u_j, u_{jk}, \dots, 0)$,

$\mathbf{u}_j = (u_1, \dots, u_j, u_{j+1}, \dots, u_n)^T$, and $\left(\frac{\partial u}{\partial n} \right)_j = \left[\left(\frac{\partial u}{\partial n} \right)_1, \dots, \left(\frac{\partial u}{\partial n} \right)_j, \left(\frac{\partial u}{\partial n} \right)_{jk}, \dots, \left(\frac{\partial u}{\partial n} \right)_n \right]^T$, where

$j = 1, \dots, n-1$. Thus, from the integrals in equations (2.12), and (2.13) we can write

$$\int_{\Gamma_{e_j}} u \frac{\cos(r,n)}{2\pi r} d\Gamma = \mathbf{F}_{ij} \cdot \mathbf{u}_j, \text{ and } \int_{\Gamma_{e_j}} \frac{\partial u}{\partial n} \frac{1}{2\pi} \ln \frac{1}{r} d\Gamma = \mathbf{D}_{ij} \cdot \left(\frac{\partial u}{\partial n} \right)_j, \quad (2.24)$$

where $1 \leq i \leq n$, $1 \leq j \leq n-1$, $k = j+1$.

Hence, the sum of these integrals is given by (in vector form):

$$\begin{aligned} \sum_{l=1}^n \int_{\Gamma_{e_l}} u \frac{\cos(r,n)}{2\pi r} d\Gamma &= (F_{i1}, \dots, F_{il}, \dots, F_{in}) \cdot (u_1, \dots, u_l, \dots, u_n)^T \\ &= \sum_{l=1}^n F_{il} u_l = \mathbf{F}_i \cdot \mathbf{u}, \end{aligned} \quad (2.25)$$

$$\sum_{l=1}^n \int_{\Gamma_{e_l}} \frac{\partial u}{\partial n} \frac{1}{2\pi} \ln \frac{1}{r} d\Gamma = (D_{i1}, \dots, D_{il}, \dots, D_{in}) \cdot \left[\left(\frac{\partial u}{\partial n} \right)_1, \dots, \left(\frac{\partial u}{\partial n} \right)_l, \dots, \left(\frac{\partial u}{\partial n} \right)_n \right]^T$$

$$= \sum_{l=1}^n D_{il} \left(\frac{\partial u}{\partial n} \right)_l = \mathbf{D}_i \cdot \frac{\partial \mathbf{u}}{\partial \mathbf{n}} \quad (2.26)$$

where F_{il} and D_{il} are the sum of f_{il} and d_{il} , respectively, of the elements around a node l , given by equations (2.13) and (2.12), respectively. For node i , we can thus rewrite equation (2.9) as

$$\frac{\omega_i}{2\pi} u_i = \mathbf{F}_i \cdot \mathbf{u} + \mathbf{D}_i \cdot \frac{\partial \mathbf{u}}{\partial \mathbf{n}}. \quad (2.27)$$

From all n nodes, we obtain (or assemble) a system of linear equations written in a compact vector – matrix equation as

$$\frac{\boldsymbol{\omega}}{2\pi} \mathbf{u} = \mathbf{F} \mathbf{u} + \mathbf{D} \frac{\partial \mathbf{u}}{\partial \mathbf{n}}, \quad (2.28)$$

where $\boldsymbol{\omega} = \mathbf{diag}(\omega_i)$ is an $n \times n$ diagonal matrix of values of ω_i at the $i = 1, \dots, n$ nodes. $\mathbf{F} = (F_{il})$, and $\mathbf{D} = (D_{il})$, are also $n \times n$ matrices, and \mathbf{u} and $\frac{\partial \mathbf{u}}{\partial \mathbf{n}}$ are $n \times 1$ column vectors given by equations (2.24) and (2.25), respectively. Equation (2.28) can be rewritten as

$$\mathbf{D} \frac{\partial \mathbf{u}}{\partial \mathbf{n}} = (\boldsymbol{\omega}/2\pi - \mathbf{F}) \mathbf{u} \quad (2.29)$$

Hence, this is a system of linear equations whose right hand side is known; therefore, we can solve for $\frac{\partial u}{\partial n}$. Substituting u and $\frac{\partial u}{\partial n}$ at each node into equation (2.6) and then integrating it, we can solve for u at any point $q \in \Gamma$, from values of u given inside the domain Ω .

2.4 Boundary element solution of a boundary value problem for the Laplace equation using linear boundary elements

Consider the following boundary value problem for the 2-D Poisson's equation

$$\Delta u(x) = -2, \quad x \in \Omega \quad (2.30)$$

$$u(x) = 0, \quad x \in \Gamma \quad (2.31)$$

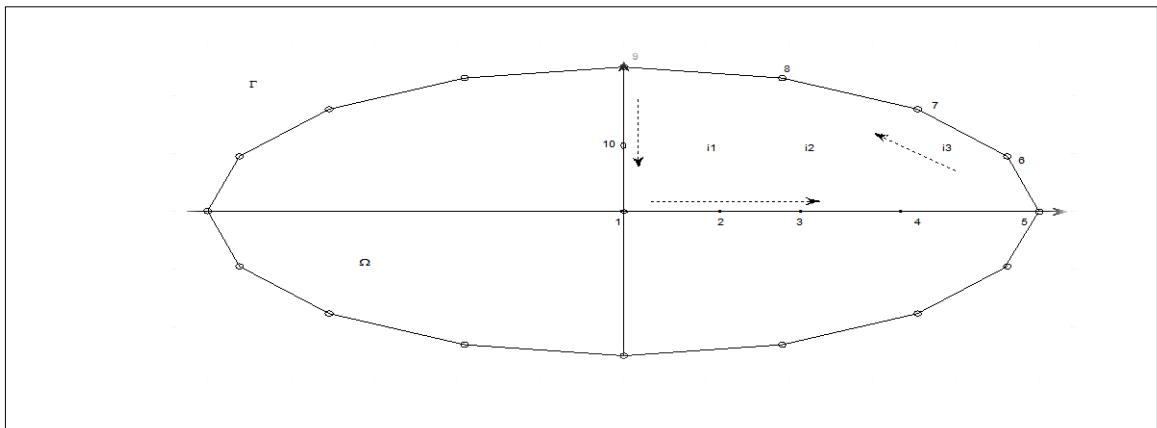
where $x = (x, y)$ and the boundary of Ω (Γ) is an ellipse (figure 2.6) given by the equation

$$\frac{x^2}{a^2} + \frac{y^2}{b^2} = 1 \quad (a = 10, b = 5). \quad (2.32)$$

Equation (2.30) is used in the study of incompressible viscous fluid flow as it flows steadily through a cylindrical pipe with an elliptical cross section. The velocity distribution in the pipe can be approximated using the BEM method [Chen, N 1991]. Using symmetry (since the flow is steady throughout the cross section of domain Ω) only the first quarter of the elliptical domain in the first quadrant of the x - y axis is used where the boundary element model consists of ten two noded linear boundary elements, and three selected internal nodes. The fact that the fluid velocity is steady throughout the pipe cross-section, and the symmetry of the pipe justifies the use of the symmetry for this problem. For steady fluid flow through out the cross-section of the pipe, the distribution of fluid velocity values at points that are symmetric with respect to an x - y

coordinate plane with origin at the center of the elliptical cross-section of the pipe, should be practically the same.[Milne-Thompson 1960].

Figure 2.6: From symmetry about the x and y axes only the upper right quarter boundary of the elliptical domain Ω is discretized where the elliptical boundary of domain Ω is given by equation (2.31)



In figure 2.6 the direction of the arrows show the the counterclockwise node numbering scheme; i_1 , i_2 , and i_3 are the internal nodes with coordinates given in table 2.1(next few pages)

Equation (2.29) is a Poisson's equation with boundary condition given by (2.30) and can be reduced to Laplace's equation if we let $u = u^* - \frac{x^2+y^2}{2}$. Then the Poisson's problem is reduced to solving the equivalent Laplace's equation for the boundary value problem

$$\Delta u^*(x) = 0, \quad x \in \Omega \quad (2.33)$$

$$u^*(x) = \frac{x^2+y^2}{2}, \quad x \in \Gamma \quad (2.34)$$

Thus, to solve for u in the original boundary value problem given by equations (2.30) and (2.31) we simply substitute the solution we get for u^* in the above boundary value problem. The above Laplace's equation with the given boundary condition is solved by the boundary element method using linear boundary elements (figure 2.6).

For an incompressible viscous fluid with steady flow through the elliptical cross section of a pipe $u = 0$ at the boundary, and the exact analytical solution of the original boundary value problem as given by equations (2.30) and (2.31) is given by [Milne-Thompson, 1960]

$$u = \frac{a^2 b^2}{a^2 + b^2} \left(1 - \frac{x^2}{a^2} - \frac{y^2}{b^2}\right) \quad (2.35)$$

Then the value of u^* inside Ω is calculated using equation (2.6) i.e.

$$u_q^* = \oint_{\Gamma} \left(u \frac{\cos(r,n)}{2\pi} + \frac{\partial u}{\partial n} \frac{1}{2\pi} \ln \frac{1}{r} \right) d\Gamma, \text{ with } u_q^* \text{ instead of } u \text{ substituted into the BEM}$$

equations, where the equation for u_q rewritten for numerical implementation in a

$$\text{computer code as: } u_q^* = \sum_{j=1}^n \int_{\Gamma_{e_j}} \left[u \frac{\cos(r,n)}{2\pi r} + \frac{\partial u}{\partial n} \frac{1}{2\pi} \ln \frac{1}{r} \right] d\Gamma$$

$$= \sum_{j=1}^n \left[\frac{L}{2\pi} \frac{\cos(r_{qj},n)}{r_{qj}} \mathbf{u}_j + \frac{L}{2\pi} \left(\frac{\partial u}{\partial n} \right)_j \frac{1}{2\pi} \ln \frac{1}{r_{qj}} \right]$$

$$= \sum_{j=1}^n \left[F_{qj} u_j + D_{qj} \left(\frac{\partial u}{\partial n} \right)_j \right],$$

where q is an interior point in domain Ω (it can also be a boundary point of the domain in case we need to determine unknown values of the function in between nodes). Results are tabulated next in the following tables. The code to calculate the solution and the errors against the exact solution are implemented in a Fortran computer code [Berbbia and Dominguez 1992]. The data inputs for the nodes, and results following tables. Values calculated by the boundary element method for the original boundary value problem given by (2.30) and (2.31) are displayed along with the exact solution and the relative errors for the displayed boundary nodes (tables 2.2, and 2.3).

Table 2.1. Input data for 10 linear boundary element nodes (figure 2.6).

Node i : (x_i, y_i)	$x_i =$	$y_i =$
(x_1, y_1)	0.0000	0.0000
(x_2, y_2)	1.2500	0.0000
(x_3, y_3)	2.5000	0.0000
(x_4, y_4)	7.5000	0.0000
(x_5, y_5)	10.0000	0.0000
(x_6, y_6)	8.8140	2.3617
(x_7, y_7)	6.1740	3.9333
(x_8, y_8)	3.3044	4.7191
(x_9, y_9)	0.0000	5.0000
(x_{10}, y_{10})	0.0000	2.5000
$(x_{11}, y_{11}) = (x_1, y_1)$	0.0000	0.0000

Next (table 2.2), denote a boundary condition indicator by **Code(i)=0**. This means that the velocity is known at node i , and **Code(i)=1** signifies that the line of symmetry is

at node i . Two values of **Code**, and two boundary conditions are read per element, corresponding to the two nodes of a linear boundary element for which the nodes are at the element. The velocity at node i given by the boundary condition in equation (2.34).

Table 2.2. Results calculated by the BEM method for boundary value problem given by (2.30), and (2.31), of the velocity distribution in a quarter of the cross-section of the elliptical domain specified by equation (2.32) for this problem.

Boundary nodes:	-----	Velocity u (BEM)	Velocity u (EXACT)	% ERROR
$x=$	$y=$	-----	-----	-----
0.0000	0.0000	20.011	20.000	0.06
2.5000	0.0000	18.758	18.750	0.04
5.0000	0.0000	15.006	15.000	0.04
7.5000	0.0000	8.7520	8.7500	0.02
10.000	0.0000	0.0000	0.0000	0
8.8140	2.6357	0.0000	0.0000	0
6.7140	3.9333	0.0000	0.0000	0
3.3044	4.7191	0.0000	0.0000	0
0.0000	5.0000	0.0000	0.0000	0
0.0000	2.5000	15.007	0.0000	0.05
0.0000	0.0000	20.011	20.000	0.06
0.0000	3.375	10.892	10.887	0.05

In table 2.2 above, note that we list the prescribed velocity distribution on the boundary of the ellipse given by equation (2.33). The velocity is not zero in the discretized boundary of the ellipse along the x and y axes in the first quadrant of the x - y plane. For the whole pipe the velocity distribution is the same for the entire cross-section of the ellipse as well as on its boundary (by symmetry).

Table.2.3: Results for the velocity distribution in the pipe for given internal nodes.

$x_{int.}$	$y_{int.}$	BEM	EXACT	%ERROR
internal node	internal node	-----	-----	-----
i1=2.5000	2.5000	13.577	13.750	0.05%
i2=5.0000	2.5000	10.005	10.000	0.05%
i3=7.5000	2.5000	3.749	3.750	0.03%

The example of a boundary value problem for the Poisson's equation discussed in this section also shows that if the equation can be reduced to a much easier Laplace's equation, then by making a substitution for a particular solution of the Poisson's equation, it can be set up in a form that can be efficiently handled numerically by a BEM analysis of the equation involving only a boundary mesh (a 1-D mesh for a 2-D boundary value problem). Of course, care should be taken to transform the boundary conditions accordingly.

2.5 Quadratic boundary elements

Next, we examine quadratic interpolation across each boundary element. Three successive nodes are used to construct each element (figure 2.7). The interpolation functions are given in isoperimetric form by:

$$u = \sum_{l=j}^{j+k} N_l u_l, \quad \frac{\partial u}{\partial n} = \sum_{l=j}^{j+k} N_l u_l,$$

$$x = \sum_{l=j}^{j+k} N_l x_l, \quad y = \sum_{l=j}^{j+k} N_l y_l,$$

$$j = 1, \dots, n - 1, k = 2. \quad (2.36)$$

In the above equations $k = 2$, means the second node in between the three noded quadratic element under analysis.

The quadratic basis and shape functions in the above equations are given by

$$N_j(\xi) = 2\xi^2 - 3\xi + 1,$$

$$N_{j+1}(\xi) = -4\xi^2 + 4\xi, \text{ and}$$

$$N_{j+2}(\xi) = 2\xi^2 - \xi. \quad (2.37)$$

The characteristics of the basis functions are:

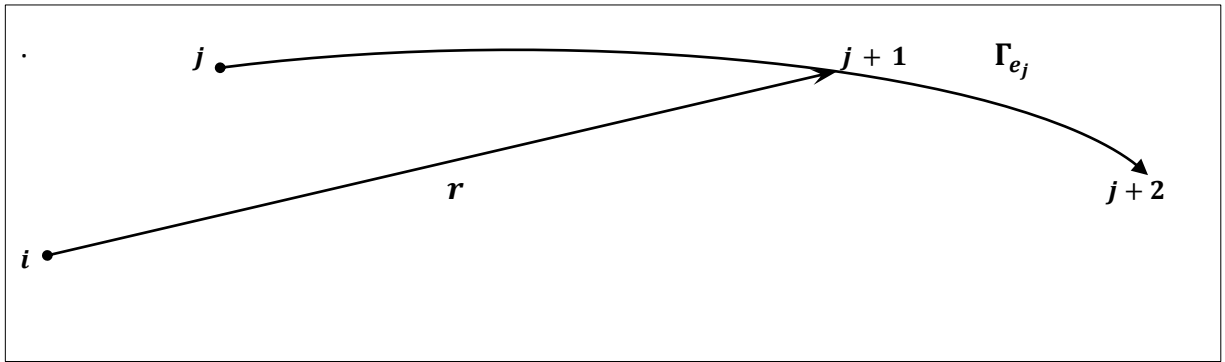
N_j, N_{j+1} , and N_{j+2} are quadratic functions of ξ , and satisfy the relations:

$$\sum_{l=j}^{j+k} N_l = 1; N_l(\xi_k) = \delta_{lk} \text{ (the Kronecker delta function)} \quad (2.38)$$

where $j = 1, \dots, n - 1$, is the number of quadratic boundary elements and $n = 2$ nodes at the endpoints of each element, and $\xi = \xi_k$, is the coordinate parameter of the isoperimetric element, and the equations in (2.38) are the Lagrange interpolation

quadratic polynomials used for second order approximation across each boundary element denoted by Γ_{e_j} where $\xi_j = 0$, $\xi_{j+1} = \frac{1}{2}$, $\xi_{j+2} = 1$. We show only a portion of the boundary (figure 2.7) over which the integration is to be carried out. The whole boundary is, of course, a closed curve.

Figure 2.7: A quadratic boundary element Γ_{e_j} ($l = j, \dots, j + k$) with its three nodes $j, j + 1, j + 2$ shown. These are its integration points; \mathbf{r} is the position vector from an internal point i of a closed region Ω to some point on the element



The integrals over each element are

$$f_{ij} = \int_{\Gamma_{e_j}} N_l(\xi) \frac{\cos(r, \mathbf{n})}{2\pi r} d\Gamma = \sum_{q=1}^4 N_l(\xi_q) \frac{\cos(r_{iq}, \mathbf{n})}{2\pi r_{iq}} L(\xi_q) \omega_q,$$

$$d_{ij} = \int_{\Gamma_{e_j}} N_l(\xi) \frac{1}{2\pi} \ln \frac{1}{r} d\Gamma = \sum_{q=1}^4 N_l(\xi_q) \frac{1}{2\pi} \ln \frac{1}{r_q} L(\xi_q) \omega_q, 1 \leq j \leq n - 1.$$

And,

$$L(\xi) = \left(\left(\sum \frac{dN_l}{d\xi} x_l \right)^2 + \left(\sum \frac{dN_l}{d\xi} y_l \right)^2 \right)^{1/2} =$$

$$= \{[4\xi - 3)x_j + (-8\xi + 4)x_k + (4\xi - 1)x_m]^2 + [4\xi - 3)y_j + (-8\xi + 4)y_k + (4\xi - 1)y_m]^2\}^{\frac{1}{2}}. \quad (2.39)$$

Note that in equation (2.39) L is a function of the quadratic element parameter ξ since the quadratic shape functions, and hence their derivatives, as well as the coordinates of a point on the isoperimetric boundary element, are functions of this parameter in the right hand side of (2.39) when we use isoperimetric boundary elements.

The remainder of the process that is needed for the quadratic element is the same as the linear element and is thus omitted from further discussion.

2.6 Solution of the Laplace equation using quadratic boundary elements

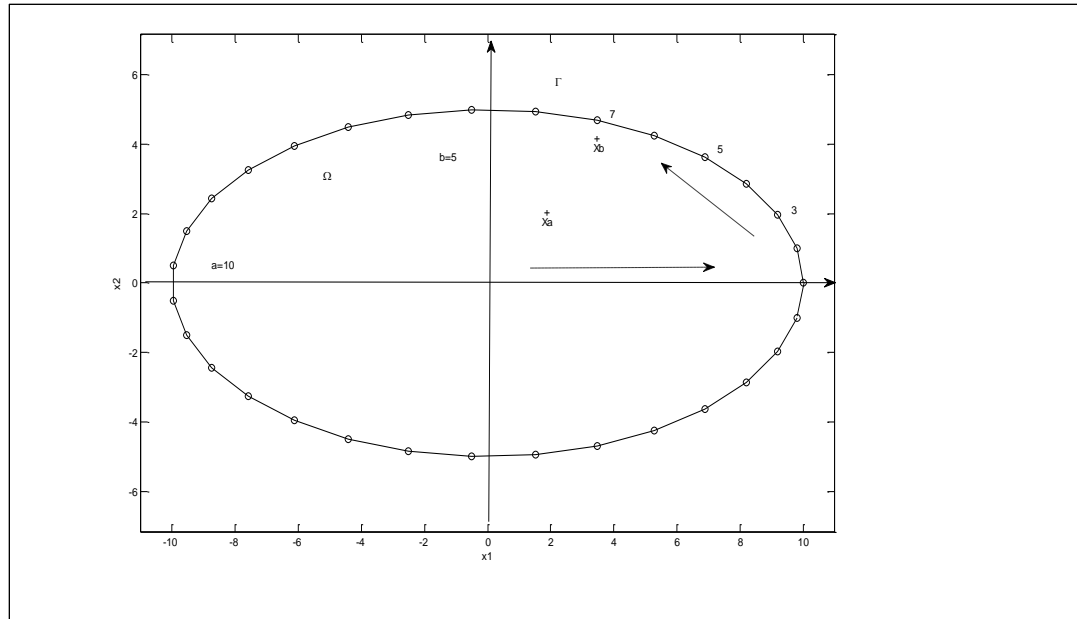
As another example of the use of the BEM to problems in potential theory, consider the problem of a prismatic bar under torsion, also known as the St. Venant's torsion problem in applied engineering mechanics to problems of stress, shear, etc,. The bar has an elliptical cross-section with semi-major axis $a=10$, and semi-minor axis $b=5$ is discretized into 16 quadratic boundary elements numbered as shown in the first quadrant (figure 2.8). Using the symmetry of the problem we calculate ϕ the so-called warping function, a measure of how much the bar is twisted under applied torsional moments or torques about its center of symmetry in the first quadrant. Using quadratic boundary element nodes, numbered in a counterclockwise fashion (figure 2.8) and supposing the St. Venant's theory of torsion applies, the strain state of a twisted bar for arbitrary cross sections, far from the points of application of the external moments,

depends very weakly on the distribution of the external load. The solution of the given problem is formulated as the following boundary value problem:

$$\Delta\phi(x_1, x_2) = 0 \text{ in } \Omega \quad (2.40)$$

$$\frac{\partial\phi(x_1, x_2)}{\partial n} = r\cos(r, t) \text{ on } \Gamma \quad (2.41)$$

Figure 2.8: Elliptical cross-section of a beam under torsional loads



The exact solution for the torsional problem involving a beam of elliptical cross section is given by $\phi = -\left(\frac{a^2-b^2}{a^2+b^2}\right) x_1x_2$ [Lebedev and Cloud 2004]. By symmetry along the axes, $\phi = 0$ inside Ω , where the harmonic function ϕ is called the warping function and $n, r,$ and t are defined for a cross section of the beam, and are the normal, position, and tangential vectors respectively, on a point of the boundary Γ of domain Ω (figure 2.8).

The displacements of the bar $u_i, 1 \leq i \leq 3$ can be found in terms of ϕ and the torsion angle per unit length θ , as follows:

$$u_1 = -\theta x_2 x_3, \quad (2.42)$$

$$u_2 = \theta x_1 x_3, \quad (2.43)$$

$$u_3 = \theta \phi, \quad (2.44)$$

where x_1 and x_2 are parallel to the principal axis and x_3 is parallel to the axis of the bar or perpendicular to the plane of this paper ; $\theta = \frac{T}{GJ}$; T is the applied torsional moment; G is the shear modulus; J is the “effective” polar moment of area, which for an elliptical cross section is given by

$$J = \frac{\pi a^3 b^3}{a^2 + b^2}. \quad (2.45)$$

The boundary value problem given by equations (2.41) and (2.42), is a Neumann type boundary value problem and has a unique solution since it can be shown that the condition

$$\oint_{\Gamma} \frac{\partial u}{\partial n} d\Gamma = 0, \quad (2.46)$$

is fulfilled with the prescribed boundary conditions. The value of ϕ in at least at one point of the domain is given in order that the solution be unique for this problem. This is

done by using the existing symmetry of the problem. For convex domains another way of stating the St. Venant's torsion theory is that for any torsion problem where the boundary is convex (as is the case for boundary value problem given by equation (2.41)) the maximum projected shear traction occurs at the point on the boundary that is nearest the centroid of the domain [Lebedev and Cloud 2004]. In our case the domain (the interior of an ellipse) is convex, and by symmetry the centroid is at the origin of axes of the ellipse . The problem is solved by using 16 quadratic elements and a computer code (Fortran) specifically desinged for quadratic interpolation over boundary element integrals. We show the results in table 2.6. Notice two internal points are used in the first quadrant of the elliptical cross-section (figure 2.8) which are marked by X_a and X_b with + (a cross sign) above them, with values shown for the input variables at nodes marked (figure 2.8) $x_3 = 3$, $x_5 = 5$ and $x_7 = 7$ (figure 2.8 and table 2.6).

Calculations show that the warping function values calculated with quadratic boudary elements are in good agreement with the exact solution. The results of the calculations are displayed next (table 2.6).

Table 2.6: Results of calculated values for warping function ϕ

Boundary and internal points used:	Calculated Warping function ϕ :	Error:	Exact:
$x_7 = (8.814, 2.361) \in \Gamma$	-12.506	-0.022	-12.484
$x_5 = (6.174, 3.933) \in \Gamma$	-14.506	-0.006	-14.570
$x_3 = (3.304, 4.719) \in \Gamma$	-9.363	-0.007	-9.356
$X_b = (4.00, 3.50) \in \Omega$	-2.399	+0.001	-2.400
$X_a = (2.00, 2.00) \in \Omega$	-8.403	-0.003	-8.400

As we can see from the results in table 2.6, using quadratic boundary elements, the calculated values of the warping function turn out to be very close to the ones calculated using the expression for exact solution for ϕ ($\phi = -\left(\frac{a^2-b^2}{a^2+b^2}\right) x_1 x_2$).

Next, we compute approximations to the solutions of the boundary value problems in this chapter using the method of fundamental solutions, or the MFS method. This method will not require a discretization of the boundary of the domain. In other words, it is essentially a meshless method[Chen 2009].

Chapter 3

Method of fundamental solutions (MFS): Comparison with the BEM for the 2-D

Poisson's and Laplace's Equations from chapter 2

3.1 Numerical Implementation of the MFS for the Poisson's equation

The main idea behind the MFS consists mainly in approximating the solution of a boundary value problem by a linear combination of known fundamental solutions associated with a set of fictitious boundary points located outside the problem domain Ω , related to the boundary value problem that we are trying to find an approximate solution too (figure 3.1). In many applications of the MFS involving 2-D boundary value problems it is common practice to generate the fictitious boundary points so that they are evenly distributed outside of the domain of the original boundary value problem [Chen 2008]. These points are part of the so-called fictitious boundary Γ^* of a 2-D domain $\Omega^* \supset \bar{\Omega}$, where $\bar{\Omega}$ denotes the closure of Ω . Likewise, Ω^* is also called a fictitious domain. We first discuss the treatment of the Laplace equation with a Dirichlet boundary condition from chapter 2. As we can recall, the problem is defined as

$$\Delta u^*(x) = 0, \quad x \in \Omega \quad (3.1)$$

$$u^*(x) = \frac{x^2 + y^2}{2}, \quad x \in \Gamma \quad (3.2)$$

We also recall that equations (3.1)-(3.2) are derived from considering a boundary value problem for the Poisson's equation in chapter 2 defined by

$$\Delta u(x) = -2, \quad x \in \Omega \quad (3.3)$$

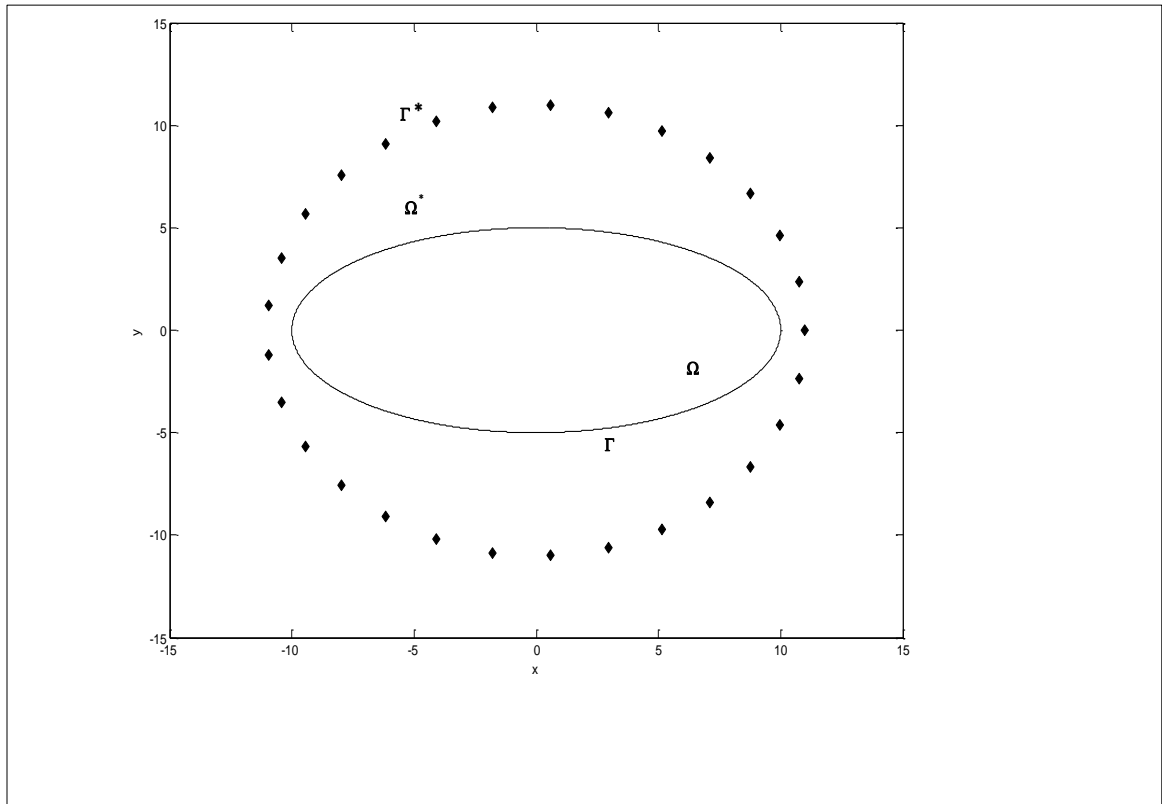
$$u(x) = 0, \quad x \in \Gamma \quad (3.4)$$

The above equation is solved indirectly by first solving the boundary value problem for unknown function u^* in the Laplace equation (3.1), with corresponding Dirichlet boundary condition given by equation (3.2). This was done in chapter 2 by the BEM method. We substitute the BEM solution for u^* into the equation

$$u = u^* - \frac{x^2 + y^2}{2} \quad (3.5)$$

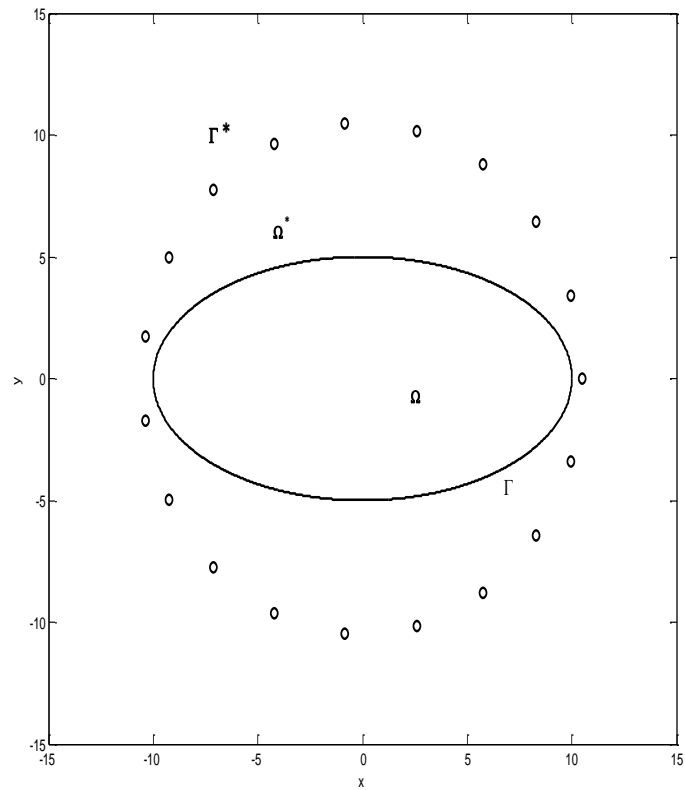
thus, we get the corresponding BEM solution to the original boundary value problem of interest (the solution u to the Poisson's equation (3.3), with boundary condition (3.4)). Equation (3.5) was used in chapter 2 to transform the boundary value problem of a Poisson's equation to the boundary value problem of the Laplace's equation. In the same vein, we treat the same boundary value problem for the Laplace equation (3.1) by the MFS method, and simply substitute the result we get using the MFS back into equation (3.4) to get the corresponding MFS solution for the original Poisson's equation given by (3.2), with boundary condition (3.3).

Figure 3.1: Geometry of the MFS. Fictitious domain Ω^* , with fictitious boundary Γ^* . A set of fictitious boundary points mark the fictitious boundary shown as dark diamonds surrounding a fictitious domain Ω^* and the domain problem Ω with boundary Γ



For the Laplace's equation in boundary value problem given by equations (3.1)-(3.2) a fictitious circular boundary Γ^* of radius $r=10.5$ is generated, and is comprised of 20 evenly distributed fictitious boundary points surrounding the boundary value problem domain defined by $\Omega = \{(x, y) \in \mathbb{R}^2 : \frac{x^2}{a^2} + \frac{y^2}{b^2} \leq 1\}$, where $a=10$, and $b=5$ (figure3.2).

Figure 3.2: Geometry of the MFS method for the Laplace's equation in boundary value problem defined by equations (3.1)-(3.2). The fictitious boundary Γ^* is marked by a set of circular blank dots as shown below, surrounding the problem domain $\Omega = \{(x, y) \in \mathbb{R}^2 : \frac{x^2}{a^2} + \frac{y^2}{b^2} \leq 1\}$ with boundary Γ (an ellipse; where $a=10$, and $b=5$)



To implement the MFS for the boundary value problem in this section we set u^* equal to

$$\widehat{u}^*(\mathbf{x}) = \sum_{j=1}^m c_j G(\mathbf{x}, \mathbf{y}_j), \quad (3.6)$$

where $\mathbf{x} = (x_i, y_i) \in \Omega$, and $\mathbf{y}_j = (x_j, y_j) \in \Gamma^*$. Then equation (3.6) defines the expression for the approximate MFS solution we seek for representing the solution of the boundary value problem given by equations (3.1)-(3.2), as a linear combination of fundamental solutions for the 2-D Laplace's equation. Thus, the MFS solution calculated by using expression (3.6) is then used to obtain an MFS approximate solution \hat{u} to the original boundary value problem involving the Poisson's equation for unknown u in (3.3). To implement the MFS by solving for the unknown coefficients c_j we use the boundary nodes $\mathbf{x} = (x_i, y_i) \in \Gamma$ corresponding to the prescribed boundary values of u^* defined by equation (3.2) and which must satisfy $u^*(\mathbf{x}) = \phi(\mathbf{x})$, for $\mathbf{x} \in \Gamma$. Thus, let

$$\widehat{u}^*(\mathbf{x}_i) = \phi(\mathbf{x}_i), \mathbf{x}_i = (x_i, y_i) \in \Gamma, \quad (3.7)$$

and for $\mathbf{y}_j = (x_j, y_j) \in \Gamma^*$, also let

$$\widehat{u}^*(\mathbf{x}_i) = \sum_{j=1}^m c_j G(\mathbf{x}_i, \mathbf{y}_j), 1 \leq i \leq m, \quad (3.8)$$

Thus, from equation (3.8), a system of linear equations for unknown coefficients c_j is obtained for the MFS expression in (3.6) that is used to obtain an approximate solution of the Laplace equation for the boundary value problem of interest in this section. The system of linear equations in (3.8), can be expressed in matrix form as

$$\begin{bmatrix} G(x_1, y_1) & \cdots & G(x_1, y_m) \\ \vdots & \ddots & \vdots \\ G(x_m, y_1) & \cdots & G(x_m, y_m) \end{bmatrix} \begin{bmatrix} c_1 \\ \cdot \\ \cdot \\ c_m \end{bmatrix} = \begin{bmatrix} \phi(x_1) \\ \cdot \\ \cdot \\ \phi(x_m) \end{bmatrix} \quad (3.9)$$

or $Ac = b$, where $A = [G(x_i, y_j)]$ is an $m \times m$ matrix with entries $G(x_i, y_j)$ (the fundamental solution of the 2-D Laplace equation computed at points given at the boundary of the problem domain, and fictitious domain), and c is the column vector consisting of the coefficients $c_j, 1 \leq j \leq m$, in equation (3.8), b is a column vector given by the right hand side of equation (3.9), consisting of entries $\phi(x_i)$, corresponding to the prescribed boundary conditions given by the right hand side of equation (3.7,) i.e. the term $\phi(x)$, where $x = x_i = (x_i, y_i) \in \Gamma, 1 \leq i \leq m$. Only the first 10 points generated for the fictitious boundary are listed next (table 3.1). By the symmetry of the problem the other 10 points generated are the same up to a change in +/- signs, although the fundamental solution of the Laplace equation is computed at all 20 points involving the fictitious boundary Γ^* , and the boundary Γ of domain Ω .

Table 3.1: The set of first $j=1, \dots, 10$, fictitious boundary points $(x_j, y_j) \in \Gamma^*$ are listed below, where Γ^* is a circle of radius $r=10.5$. The actual number of points generated was 20 for the computation of the MFS approximate solution

Γ^* is a circle of radius: $r=10.5$	$(x_j, y_j) \in \Gamma^* =$	(10.5,0.0)	(9.931,3.409)	(8.286,6.449)	(5.743,8.790)
		(2.557,10.178)	(-0.867,10.461)	(-4.217,-9.615)	(-7.111,7.725)
				(-9.234,4.997)	(-10.356,1.728)

The set of coefficients $\{c_j\}$ are determined from (3.9), or by $Ac = b$, where $A = [G(\mathbf{x}_i, \mathbf{y}_j)]$ is an $m \times m$ matrix, whose entries are the fundamental solution to the 2-D Laplace equation as described before, along with column vectors c and b , defined by (3.9). Hence, the coefficients c_j , in column vector c , are obtained from the matrix equation

$$c = A^{-1}b, \quad (3.10)$$

where A^{-1} is the inverse of matrix $A = [G(\mathbf{x}_i, \mathbf{y}_j)]$. Provided A is non-singular, the c_j will be unique.

Finally, solving for the coefficients c_j , we can construct the MFS approximate solution \hat{u} defined by (3.6), for u in the original Poisson's equation (3.3) by using (3.5). To estimate the magnitude of the error $e(\mathbf{x})$ in the MFS approximate solution \hat{u} at points $\mathbf{x} = \mathbf{x}_i = (x_i, y_i) \in \Omega$, we set $e(\mathbf{x})$ equal to

$$e(\mathbf{x}) = |u(\mathbf{x}) - \hat{u}(\mathbf{x})|, \quad (3.11)$$

where $u(\mathbf{x})$ in (3.11) is the exact solution to the Poisson's equation (3.3) given in Chapter 2.

The results of numerical implementation of the MFS method are listed below, along with BEM results from chapter 2 for the same Poisson's equation treated by the MFS here. The magnitude of the error as given by (3.11) is also displayed for interior table 3.2 below.

Table 3.2: Results of the MFS method compared with the BEM method (shown in order of coordinates used) for the Poisson's equation in 2-D domain $\Omega = \{(x, y) \in \mathbb{R}^2 : \frac{x^2}{a^2} + \frac{y^2}{b^2} \leq 1\}$ shown in figure (3.2). The % relative error for the BEM was shown in table (2.2)

Fictitious Boundary Γ^* (points tested)	$(x_j, y_j) \in \Gamma^* =$	(10.5, 0.0)	(9.931, 3.409)	(8.286, 6.449)	(5.743, 8.790)
(2.55, 10.178)	(-0.86, 10.461)	(-4.217, -9.615)	(-7.111, 7.725)	(-9.234, 4.997)	(-10.356, 1.728)
Domain Ω (points tested)	$(x_j, y_j) \in \Omega =$	(0.0, 0.0)	(2.5, 0.0)	(5.0, 0.0)	(7.5, 0.0)
(2.5, 2.5)	(1.25, 3.3750)	(-2.5, -2.5)	(-5.0, 0.0)	(-7.5, 0.0)	(-1.25, -3.750)
MFS approximation:	20.911	18.769	15.116	8.757	10.500
13.757	-----	-----	-----	-----	-----
BEM approximation:	20.11	18.758	15.006	8.752	10.557
13.757	no change	no change	no change	no change	no change
Exact solution:	20.00	18.750	15.00	8.750	10.755
13.750	no change	no change	no change	no change	no change
$e(\mathbf{x}) =$ (MFS: Eq.3.11)	0.911	0.019	0.116	0.005	0.056

3.2 Numerical Implementation of the MFS for the Laplace's equation with a Neumann boundary condition for the St.Venant's beam torsion problem in chapter 2

Recall the St.Venant's Torsion problem for an elliptical cross section of a bar under torsional, or "twisting" loads. For simplicity we use a 2-D domain exactly the same as the one for the Poisson's boundary value problem. A fictitious boundary Γ^* comprised of 32 fictitious boundary points is generated surrounding domain Ω . Γ^* is a circle of radius $r=11.00$. In a similar fashion as the boundary value problem for the Poisson's equation,

we take advantage of the symmetry of the problem, and the assumption of uniformly distributed loads on the cross section of the bar. Thus, it suffices to list the first $(x_j, y_j) \in \Gamma^*, j = 1, \dots, 9$, generated fictitious boundary points lying approximately in the upper right half of the x-y plane (table 3.3) and pair these with the non-fictitious boundary points $\boldsymbol{x} = (x_i, y_i) \in \Gamma$, for $1 \leq i \leq m$, and use the same exact procedure for the numerical implementation of the MFS to construct an MFS expression for an approximate solution to the the St.Venant's boundary value problem treated in this section by the MFS method. The numerical implementation of the MFS is carried over around the entire boundary using an algorithm similar to the one used for the numerical solution to the Poisson's equation. The high symmetry of the problem will yield results virtually the same as for the points we list in table 3.3 next. Only a slight modification has to be made for this problem since the boundary condition is not a Dirichlet type boundary condition. As mentioned above the boundary condition for this problem is of Neumann type. The computation of an MFS solution at various points of the problem domain employs the outward normal derivative of the fundamental solution of the Laplace equation as explained in what follows.

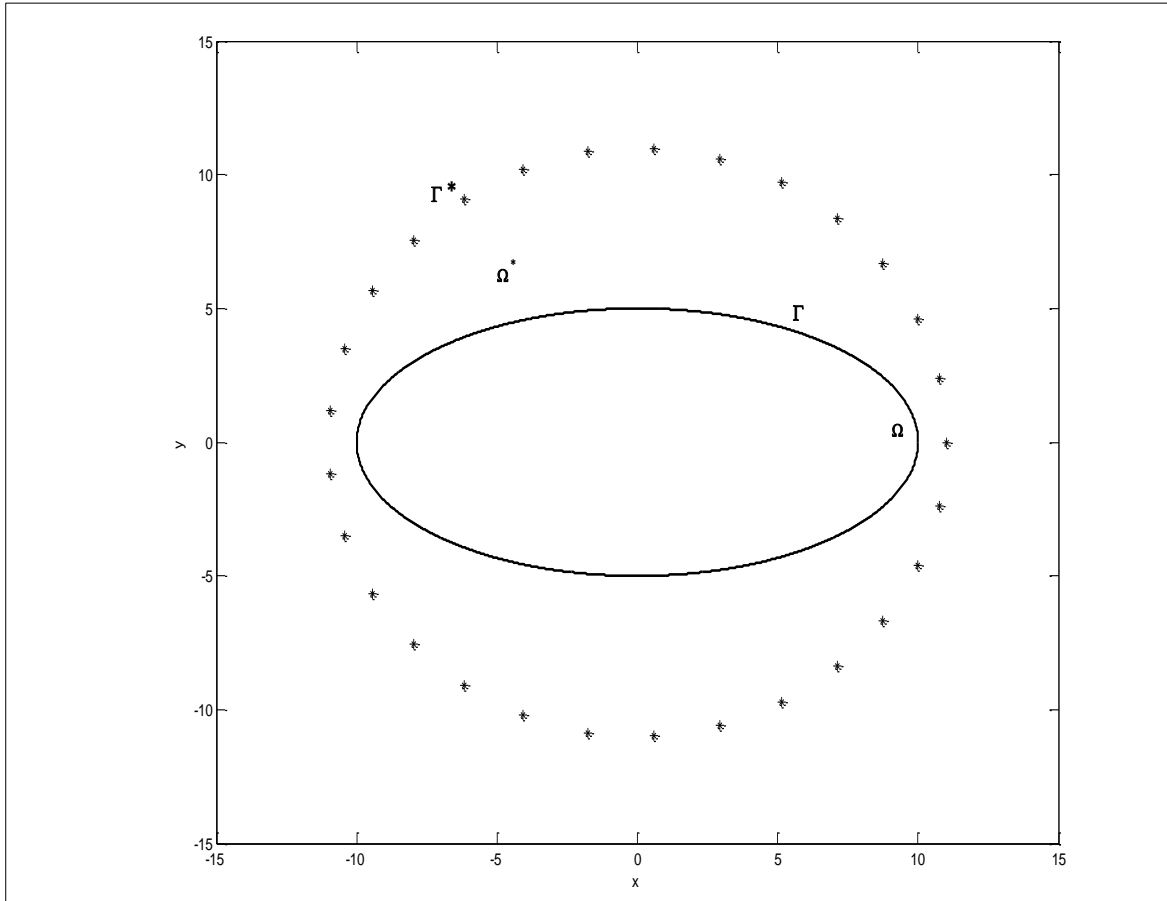
Table 3.3: Some generated fictitious boundary points $(x_j, y_j) \in \Gamma^*$ used to construct an MFS approximate solution for the St.Venant's torsion problem

$(x_j, y_j) \in \Gamma^*$ (a circle of radius $r=11.0$)
$(x_1, y_1) = (11.00, 0.00)$
$(x_2, y_2) = (10.7428, 2.6357)$
$(x_3, y_3) = (11.00, 0.00)$
$(x_4, y_4) = (8.750, 6.6559)$
$(x_5, y_5) = (7.1212, 8.3838)$
$(x_6, y_6) = (5.1225, 9.7186)$
$(x_7, y_7) = (2.9428, 10.5990)$
$(x_8, y_8) = (0.5955, 10.9839)$
$(x_9, y_9) = (-1.7796, 10.8551)$

Fictitious boundary points listed in table 3.3 are shown below (figure 3.3) marked by

dark crosses (\dagger) surrounding domain $\Omega = \{(x, y) \in \mathbb{R}^2 : \frac{x^2}{a^2} + \frac{y^2}{b^2} \leq 1\}$.

Figure 3.3: Fictitious boundary points used for the MFS treatment of the St.Venant's torsion problem. The fictitious boundary is denoted by Γ^* as shown below consisting of dark crosses surrounding domain $\Omega = \{(x, y) \in \mathbb{R}^2 : \frac{x^2}{a^2} + \frac{y^2}{b^2} \leq 1\}$



Now we implement MFS method to obtain an approximate solution to the boundary value problem for the St.Venant's torsion problem. First, we recall from chapter 2, the problem was defined as

$$\Delta\phi(x_1, x_2) = 0 \text{ in } \Omega \tag{3.11}$$

$$\frac{\partial\phi(x_1, x_2)}{\partial n} = r\cos(r, t) \text{ on } \Gamma \tag{3.12}$$

Similar to the construction of the MFS expression to approximate the solution to the Laplace's equation in section 3.1, we define an MFS expression for the solution of the Neumann type boundary value problem which takes the of expression

$$\hat{\phi}(\mathbf{x}) = \sum_{j=1}^m c_j G(\mathbf{x}, \mathbf{y}_j) \quad , \quad (3.13)$$

where $\mathbf{x} = (x, y) \in \Omega$, and $\mathbf{y}_j = (x_j, y_j) \in \Gamma^*$ are some fictitious boundary points. Using similar arguments to implement the MFS method for the Laplace's equation in section 3.1, denote by $\psi(\mathbf{x})$ the given prescribed boundary conditions (table 3.3). Hence, choose $\mathbf{x} = \mathbf{x}_i \in \Gamma$, $1 \leq i \leq m$, we set

$$\frac{\partial \hat{\phi}(\mathbf{x})}{\partial n} = \psi(\mathbf{x}_i), \quad 1 \leq i \leq m. \quad (3.14)$$

Namely

$$\psi(\mathbf{x}_i) = \sum_{j=1}^m c_j \frac{\partial G(\mathbf{x}_i, \mathbf{y}_j)}{\partial n}, \quad 1 \leq i \leq m, \quad (3.15)$$

where $\mathbf{y}_j = (x_j, y_j) \in \Gamma^*$, and $\mathbf{x}_i = (x_i, y_i) \in \Gamma$. The prescribed boundary conditions used in equation (3.14) are shown in table 3.3 next.

Table 3.3: Prescribed boundary conditions for nodes $(x_i, y_i) \in \Gamma$, in the first quadrant of the x-y plane, for quadratic boundary elements related to the St. Venant's torsion problem. Prescribed node values for four quadratic boundary elements are shown. Each element consists of $i=3$ nodes (figure 2.8)

PRESCRIBED BOUNDARY CONDITIONS	FIRST NODE $(x_i, y_i)/\text{VALUE}$ $i = 1$	SECOND NODE $(x_i, y_i)/\text{VALUE}$ $i = 2$	THIRD NODE $(x_i, y_i)/\text{VALUE}$ $i = 3$
ELEMENT Γ_j : $1 \leq j \leq 4$	*****	*****	*****
Γ_1	(10.0,0.0)/0.0	(9.670,1.273)/-3.379	(8.814,2.3617)/-4.8834
Γ_2	(8.814,2.367)/-4.8334	(7.7008,3.1898)/-4.9447	(6.174,3.933)/-4.3104
Γ_3	(6.174,3.933)/-4.3104	(4.7898,4.3891)/-3.4657	(3.3044,4.719)/-2.4411
Γ_4	(3.3044,4.719)/-2.4411	(1.557,4.939)/-1.1614	(0.00,5.00)/-0.3379

Again, by symmetry the prescribed boundary conditions the boundary elements given by table 3.3 are the same for the rest of the boundary elements around the perimeter of the elliptical boundary.

For numerical implementation of the MFS of the boundary value problem, we re-express equation (3.15) in matrix form as

$$\begin{bmatrix} \frac{\partial G(x_1, y_1)}{\partial n} & \dots & \frac{\partial G(x_1, y_m)}{\partial n} \\ \vdots & \ddots & \vdots \\ \frac{\partial G(x_m, y_1)}{\partial n} & \dots & \frac{\partial G(x_m, y_m)}{\partial n} \end{bmatrix} \begin{bmatrix} c_1 \\ \vdots \\ c_m \end{bmatrix} = \begin{bmatrix} \psi(x_1) \\ \vdots \\ \psi(x_m) \end{bmatrix}, \quad (3.16)$$

or $Ac = b$, where $A = \left[\frac{\partial G(x_i, y_j)}{\partial n} \right]$ is the matrix above in the left hand side of (3.16) with entries $\frac{\partial G(x_i, y_j)}{\partial n}$ representing the values of the outward normal derivatives of $G(x_i, y)$, computed at boundary, and fictitious boundary points, $x_i = (x_i, y_i) \in \Gamma$, and $y_j = (x_i, y_i) \in \Gamma^*$, respectively, for $1 \leq i, j \leq m$, and c is the column vector of unknown coefficients c_j , and b is the column vector of prescribed boundary values $\psi(x_i)$ for the outward normal derivatives of ϕ (the warping function) at given nodes $x = x_i \in \Gamma$ (table 3.3). As in section 3.1 to implement the MFS we compute A^{-1} , the inverse of $A = \left[\frac{\partial G(x_i, y_j)}{\partial n} \right]$ to solve for the coefficients c_j and thus use these to construct the MFS expression (3.13) for the approximate solution to the Laplace equation with Neumann boundary conditions, or the St.Venant's torsion problem, defined by (3.11)-(3.12). The computation of $A = \left[\frac{\partial G(x_i, y_j)}{\partial n} \right]$ leads to a matrix that is close to being singular. A similar result was observed for the matrix of fundamental solutions in the MFS treatment of the Laplace's equation in section 3.1. In either case, both matrices were invertible. The size the matrix of the MFS approximate solution given by $A = \left[\frac{\partial G(x_i, y_j)}{\partial n} \right]$ is a 36×36 square matrix as 16 quadratic boundary elements each with 3 nodes was used to compute A . 9 of the generated fictitious boundary nodes, are also listed. These 9 nodes cover the first four quadratic boundary elements used in chapter 2 for this problem. All located in the first quadrant of the x-y plane. Again, the computation of entries for matrix A above is actually carried out around the entire perimeter of the elliptic boundary of the domain. Finally, using some interior boundary points we compute the MFS approximate solution using (3.13). We display these results

in table 3.4 next. The magnitude of the error is computed using the relation: $e(\mathbf{x}) = |\phi(\mathbf{x}) - \hat{\phi}(\mathbf{x})|$ (similar to equation 3.11).

Table 3.4: Results of the MFS compared with the BEM (shown in order of coordinates used) for the Laplace's equation of the St. Venant's torsion problem for a beam of elliptical cross-section defined by $\Omega = \{(x, y) \in \mathbb{R}^2 : \frac{x^2}{a^2} + \frac{y^2}{b^2} \leq 1\}$. The % relative error for the BEM was shown in table (2.2) only for two interior points. Additional interior BEM points tested (not shown in table (2.2)) are also displayed

Fictitious Boundary Γ^* (points tested)	(11.00,0.00)	(10.7428,2.63)	(9.98,4.61)	(8.75,6.66)
(7.12,8.38)	(5.12,9.72)	(2.94,10.59)	(0.59,10.98)	(1.78,10.86)
Domain Ω (points tested)	$(x_j, y_j) \in \Omega =$	(1.1, 1.1)	(2.0, 2.0)	(2.5, 2.5)
(3.1, 3.1)	(4.0, 4.0)	(4.5, 3.5)	(4.5, 4.5)	(5.0, 5.0)
MFS approximation:	-0.688	-2.096	-4.6600	-7.2130
-11.8711	-3.9377	-15.1773	-15.1888	-18.7711
BEM approximation:	-0.73	-2.093	-4.6701	-7.2170
-11.8901	-3.9444	-15.1871	-15.1651	-18.68
Exact solution:	-0.75	-3.00	-4.6875	-7.2075
-12.00	-3.9375	-15.1875	-15.1875	-18.75
$e(\mathbf{x}) =$ (MFS: Eq.3.11)	0.042	0.096	0.0275	0.0211
$e(\mathbf{x}) =$ (BEM)	0.030	0.093	0.0174	0.0040

3.3 Concluding Remarks

From observation of the results obtained by application of the MFS and the BEM, to the boundary value problems treated in this thesis, both methods yielded results very close to the exact analytic solutions for the Poisson's equation in the model of an ideal fluid velocity distribution as it flows across a pipe of elliptical cross section, at a uniform rate. The results for the analysis of torsional loads over a beam of elliptical cross section with same parameters as the one used in the boundary value problem for the Poisson's equation i.e., the St.Venant's torsion problem for a beam of uniform cross section subject to external loads, also seems to lead to results very much in accord with the exact analytical solution to this problem. In contrast to the BEM, the MFS was decisively less complicated than the BEM, as much more work is involved in implementation of the BEM. Choosing how to discretize the boundary, by deciding whether linear, quadratic, or higher order interpolation functions, is only the beginning of using the BEM method. The computer implementation can be the difficult part of using the BEM, as singular integrals can may be encountered and make the computer coding involved very time consuming, as well as the actual time involved in getting results from carrying out the computations on some particular computing device. The BEM is still however a better alternative to say FEM methods involving even more time discretizing a problem domain, in addition to the time involved in the construction of an appropriate computer code for the numerical implementation of a problem to which the BEM may be equally suitable to handle [Brebbia 1992]. Application of the MFS to the same problems treated in this thesis paper was again a little much easier than the BEM. One obvious reason was

the use of a few sets of points on a so-called fictitious boundary surrounding the domain of interest. Thus, no time is spent on figuring out how to discretize the boundary of the problem domain. The computer coding for numerically implementing this method for the same problems was less time consuming also as one does not have to worry about the many aspects of the geometry of the domain being treated, which could in itself make discretizing difficult a boundary if the geometry of the domain is highly irregular. No boundary discretizing involved was especially a nice feature of using the MFS for the boundary value problems treated in this thesis paper. Generating solutions for by the MFS took less computer time than generating them by the BEM method. This was mainly due to the coding involved for the algorithms to compute the fundamental solutions of the 2-D Laplace equation. In the BEM the computer coding of the algorithms used in the numerical implementation of the problems treated to handle the specific problems discussed in this thesis paper is considerably more involved. Besides computing the fundamental solution, many integrals over the boundary elements have to be computed. In short more time and computational resources are considerably more demanding issues in using the BEM in contrast to the MFS. In either case, from tables 3.2 and 3.4 of this chapter displaying results for both methods, one can see that both methods however different from each other seem to show little variation in results they yield, and approximate the exact analytical solutions to both boundary value problems to which they were applied too.

In both boundary value problems studied in this thesis the geometry of an ellipse is obviously highly symmetrical and so choosing a fictitious boundary such as a circle was

the most obvious choice to work with for the numerical implementation of the MFS for both problems. However, it should be noted that the MFS seems to be best applicable to partial differential equations with known fundamental solutions. In many cases finding the fundamental solution to some particular partial differential equation can be quite difficult depending on how singular the integrals involved in computing such solutions may be [Chen and Smyrlis 2008]. The accuracy of the MFS also seems to depend on how well the collocation, and or source points of a fictitious domain are distributed over the fictitious boundary surrounding the problem domain [Li and Chen 2009]. For the particular problems studied here however, this did not seem to be a problem as long as a circular boundary with not too large of a radius or too small of a radius was used. Only a couple of two other radii were tested to see if results yielded would get any better. But it made little difference for both boundary value problems studied for this thesis paper. As long as the radii of fictitious circular boundaries did not vary much from the ones chosen originally, the matrices constructed to solve for the the coefficients in the MFS approximate solutions, given by equations (3.8), and (3.15) for the MFS approximate solution of the Laplace's equation (then for the Poisson's equation), and for the St. Venant's torsion problem, respectively, though highly close to being singular, produced results for the Laplace's equation related to the Poisson's equation, and the St. Venat's torsion problem, show fairly good results in very good agreement with the exact analytical solutions. Again, a look results displayed in tables 3.2, and 3.4 confirms this. To complement numerical results in these tables, a 3-D plot displaying the MFS solution to the Poisson's boundary value problem of fluid flow

through the cross-section of an elliptical pipe is shown next (figure 3.4). In addition, a 2-D, and 3-D plot for the St.Venant's torsion problem is shown, displaying the distribution of torsional loads over the cross-section of the same type of geometry as the Poisson's problem of fluid flow distribution through the pipe as discussed earlier(elliptical cross section, see figures 3.5 and 3.6).

Figure 3.4: 3-D plot showing velocity distribution of fluid across a pipe of elliptical cross-section for the Poisson's equation (MFS approximate solution).The arrows show the direction of the flow. Note the small arrows near the boundary of the pipes cross section to depict velocity drop until near zero velocity conditions prevail on the boundary where the prescribed boundary conditions are of zero velocity

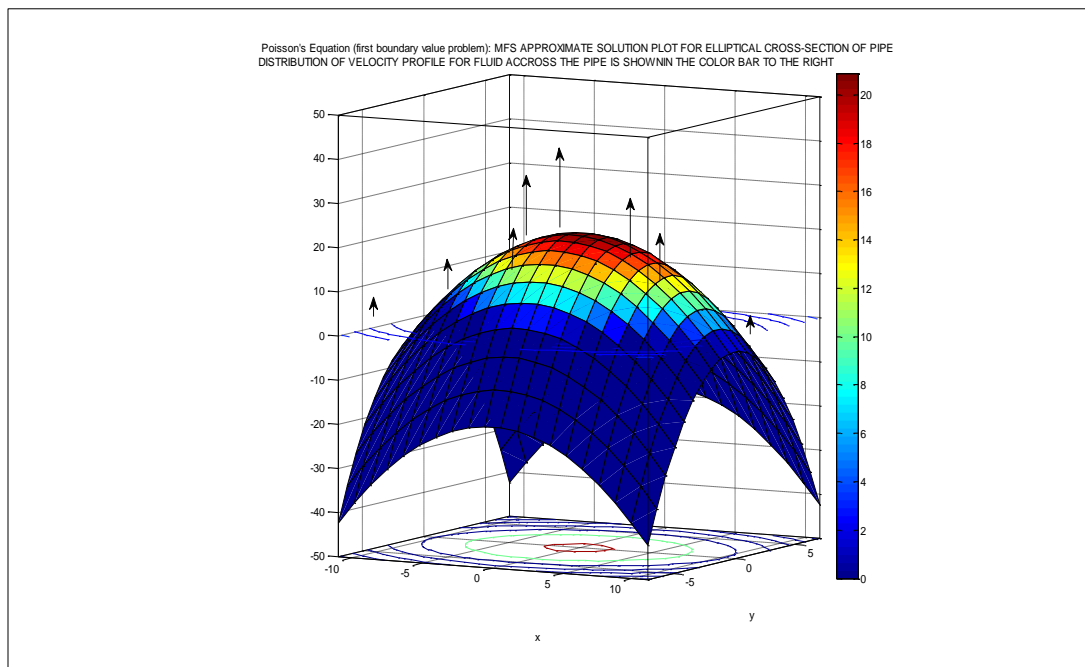


Figure 3.5: 2-D plot of torsional load distribution (MFS approximation) over the elliptical cross-section of a beam for the St.Venant's torsion problem. The cross-like area shows the region of the cross-section of the beam towards where the maximum projected tractions tend to concentrate on part of the beams cross-sectional area closest to the centroid of the beam. The centroid of the beam is clearly just the origin of axes in the x-y plane

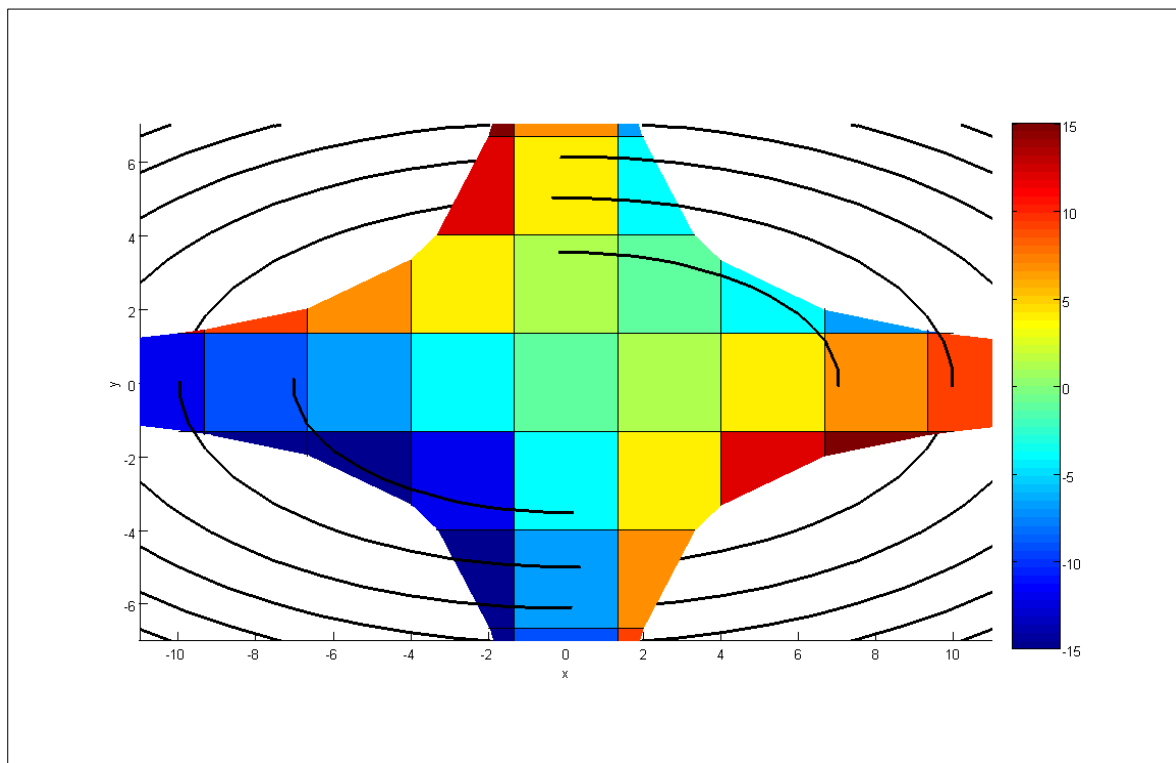
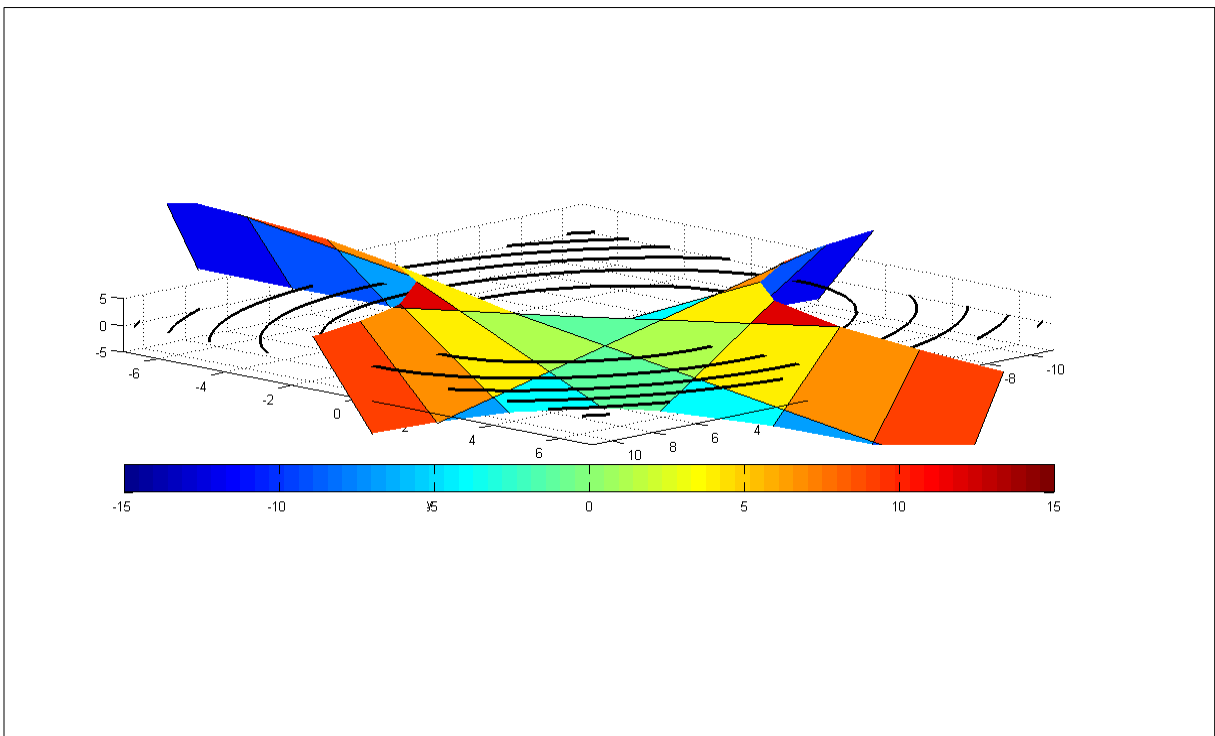


Figure 3.6: A 3-D plot of a small slice of the elliptical beam shown in figure 3.6 showing the distribution of shear stress when the beam is twisted.(MFS approximation). The contours shown in black are part of the region of the beams cross section. The surface intersecting these contours represents the shear stress distributions mostly concentrated near the beams centroid as discussed in Chapter 2



APPENDIX A

LIST OF ABBREVIATIONS

2-D	two-dimensions
BEM	boundary element method
FEM	finite element method
MFS	method of fundamental solutions
PDE	partial differential equations

APPENDIX B

LIST OF FIGURES

1.1	The 2-D δ function.....	3
1.2	Small disk Γ_ϵ enclosing point p within domain Ω	4
1.3	Point p on a smooth boundary of a domain Ω as the center of a small disk Γ_ϵ	5
1.4	Point p on a broken boundary of domain Ω as the center of small disk Γ_ϵ	7
1.5	A 2-D domain Ω with boundary $\partial\Omega$	9
2.1	A 2-D elliptical domain in the x-y plane.....	14
2.2	Point q on a smooth 2-D boundary of domain Ω subtending angle ω_q	18
2.3	Linear boundary element on a 2-D domain Ω	19
2.4	A singular linear boundary element with outward unit normal n	24
2.5	Singular linear boundary element with a fixed quadrature point.....	25
2.6	2-D domain Ω . An ellipse with a quarter of its boundary discretized by 5 nodes....	29
2.7	An example of a quadratic boundary element.....	36
2.8	Elliptical cross section of a beam for the St.Venant's torsion problem.....	38
3.1	Geometry of the MFS. A fictitious boundary Γ^* surrounding a 2-D domain Ω	44
3.2	MFS geometry for solution of the 2-D Laplace equation of fluid flow.....	45
3.3	MFS geometry for the St.Venant's torsion problem.....	52
3.4	MFS 3-D plot for the Poisson's equation of fluid flow.....	60
3.5	2-D plot for the St.Venant's torsion problem.....	61
3.6	3-D plot for the St.Venants's torsion problem.....	62

REFERENCES

- [1] C.A. Brebbia and J. Dominguez. Boundary Boundary Elements An Introductory Course. Computational Mechanics Publications McGraw-Hill Book Company, 1992.

- [2] C.S. Chen, Y.S. Smyrlis. The Method of Fundamental Solutions A Meshless Method. Dynamic Publishers Inc., 2008.

- [3] Debanath, L. and Mikusinsky, P. Introduction to Hilbert Spaces with Applications, Fifth Edition. Academic Press, Boston, 2005.

- [4] Jichun Li, Yi-Tung Chen . Computational Partial Differential Equations Using Matlab. CRC Press, 2009.

- [5] Lebedev P. L. and Cloud J.M. Approximating Perfection. A Mathematician's Journey into The World of Mechanics. Princeton University Press, 2004

- [6] Milne-Thomson, L.M. Theoretical Hydrodynamics. The Macmillan Company, New York, 1960.

VITA

Graduate College
University of Nevada, Las Vegas

Ermes Anthony Salgado-Ibarra

Home Address:

965 Cottage Grove Avenue Apt.40
Las Vegas, Nevada 89119

Degrees:

Bachelor of Science, Applied Mathematics, 2004
UCLA, University of California, Los Angeles

Thesis Title:

The Method of Fundamental solutions. A Meshless method approach to the numerical solution of the 2-D Poisson's, and Laplace's equation comparison and contrast to the boundary element method

Thesis Examination Committee:

Chairperson, Dr. Xin Li, Ph.D.
Committee Member, Dr. Amei Amei Ph.D.
Committee Member, Dr. Monika Neda, Ph.D.
Graduate Faculty Representative, Dr. Pushkin Kachroo, Ph.D.

